



Geochemical characterization of the siliciclastic rocks of Chitravati Group, Cuddapah Supergroup: Implications for provenance and depositional environment

V SOMASEKHAR¹, S RAMANAIAH² and D SRINIVASA SARMA^{1,*}

¹*CSIR-National Geophysical Research Institute, Uppal Road, Hyderabad 500 007, India.*

²*Department of Geology, Sri Venkateswara University, Tirupati 517 502, India.*

*Corresponding author. e-mail: dssarma@ngri.res.in

MS received 11 July 2017; revised 16 September 2017; accepted 23 September 2017; published online 23 May 2018

Petrological and geochemical studies have been carried out on Pulivendla and Gandikota Quartzite from Chitravati Group of Cuddapah Supergroup to decipher the provenance and depositional environment. Both the units are texturally mature with sub-rounded to well-rounded and moderately to well-sorted grains. Majority of the framework grains are quartz, in the form of monocrystalline quartz, followed by feldspars (K-feldspar and plagioclase), mica, rock fragments, heavy minerals, with minor proportion of the matrix and cement. Based on major element geochemical classification diagram, Pulivendla Quartzite is considered as quartz-arenite and arkose to sub-arkose, whereas Gandikota Quartzite falls in the field of lith-arenite and arkose to sub-arkose. Weathering indices like CIA, PIA, CIW, ICV, Th/U ratio and A–CN–K ternary diagram suggest moderate to intense chemical weathering of the source rocks of these quartzites. Whole rock geochemistry of quartzites indicate that they are primarily from the first-cycle sediments, along with some minor recycled components. Also their sources were mostly intermediate-felsic igneous rocks of Archean age. The tectonic discrimination plots, Th–Sc–Zr/10 of both these formations reflect active to passive continental margin setting. Chondrite-normalized rare earth element (REE) patterns, and various trace element ratios like Cr/Th, Th/Co, La/Sc and Th/Cr indicate dominantly felsic source with minor contribution from mafic source. Th/Sc ratios of Pulivendla and Gandikota Quartzite are in close proximity with average values of 2.83, 3.45 respectively, which is higher than AUCC (Th/Sc = 0.97), demonstrating that the contributions from more alkali source rocks than those that contributed to AUCC.

Keywords. Cuddapah Basin; Chitravati Group; Pulivendla and Gandikota Quartzite; geochemistry; provenance.

1. Introduction

Geochemical studies of clastic sedimentary rocks reveal the source area, tectonic setting of the basin and in addition provides insights into the paleogeographic, chemical environment of deposition (Bhatia and Crook 1986; Roser and Korsch 1986, 1988;

Erickson *et al.* 1992; Cullers and Podkovyrov 2000; Condie *et al.* 2001; Absar *et al.* 2009; Absar *et al.* 2016; Khan and Khan 2015, 2016) and helps to estimate weathering intensity and paleoclimate (Bhatia 1983; Bhatia and Crook 1986; Roser and Korsch 1986, 1988; McLennan *et al.* 1990). The geological processes leave characteristics in the form of

geochemical signatures making sedimentary rocks as the most important repository of geochemical data available for the reconstruction of ancient earth surface environment (Sageman and Lyons 2005). Petrography, which includes modal abundances of minerals and textural analysis, is important; however, due to some inherent advantages of geochemistry later became a valuable tool. Studies of major oxides, selected trace elements and rare earth elements (REEs) including LREE and HREE and their ratios are sensitive indicators for provenance and tectonic settings (Bhatia 1983; Bhatia and Crook 1986; Roser and Korsch 1986, 1988; McLennan and Taylor 1991; Condie 1993; Nesbitt and Young 1996; Cullers and Podkovyrov 2002). The La and Th are immobile elements and are found in higher proportion in felsic source whereas, concentration of trace elements like Co and Sc are higher in mafic igneous source (Taylor and McLennan 1985; Wronkiewicz and Condie 1987). Therefore, higher values of Th/Sc, Th/Co and La/Sc display crustal derivation and lower values indicate a mantle source. The aim of this study is to estimate the geochemical discriminations among two different formations of Chitravati Group of Cuddapah Supergroup and to understand their source characteristics, paleoclimatic conditions and tectonic setting.

2. General geology of study area

The crescent-shaped intra-cratonic Cuddapah basin extends for about 440 km in length along its eastern margin and 145 km diagonally in its widest part (Nagaraja Rao *et al.* 1987). It is a foreland basin in front of the Eastern Ghat Mobile Belt (EGMB; Dasgupta *et al.* 2005; Saha and Patranabis-Deb 2014; Matin 2015). Cuddapah sediments rest on the Archeans (~2520 Ma; Jayananda *et al.* 2008) and many of the schist belts also form basement (i.e., Veligallu, Kadiri, Penakacherla, Gadwal, etc., King 1872; Nagaraja Rao *et al.* 1987; figure 1). The grade of metamorphism increases from west to east during the Middle to Late Proterozoic Eastern Ghat Orogeny (Goodwin 1996). The Cuddapah basin contains sedimentary piles belonging to Paleo-Mesoproterozoic Cuddapah Supergroup and Meso-Neoproterozoic Kurnool Group. A major unconformity separates the Cuddapah Supergroup from the overlying Kurnool Group. The Cuddapah Supergroup consists of Papaghni, Chitravati, Nallamalai

groups and Srisailam Quartzite. All these units are separated by the unconformities which show variable environment of deposition (Saha and Tripathy 2012; figure 2). Kurnool Group is followed by Banganpalli Quartzite, Narji Limestone, Owk Shale, Paniam Quartzite, Koilkuntla Limestone, and Nandyal Shale. On the basis of sediment characteristics, spatial distribution and evolution of the basin through time, Nagaraja Rao *et al.* (1987) identified four sub-basins within the Cuddapah Basin (Papaghni sub-basin, Kurnool sub-basin, Srisailam sub-basin and Palnad sub-basin). Papaghni sub-basin consists of Papaghni and Chitravati Group. Papaghni Group consists of Gulcheru and Vempalle formations. Gulcheru Formation comprises conglomerate and quartzite (figure 2) (2502 ± 17 Ma; Nagaraja Rao *et al.* 1987; Chakrabarti *et al.* 2009; Basu *et al.* 2014; Collins *et al.* 2015) and Vempalle Formation is predominantly carbonate succession containing dolomites (1752 ± 41 Ma; Zachariah *et al.* 1999), shale, quartz arenite, chert, basic flows and sills. Basal unit of dolostones are uranium-bearing dolomites/calcareous arenite, forms part of the Vempalle Formation (Absar *et al.* 2016, reference therein). Chitravati Group, disconformably overlies the Papaghni Group, which is comprised of alternate sequences of arenaceous, argillaceous lithounits, basic sills and tuffs. These lithounits together form Pulivendla Quartzite, Tadpatri Formation and Gandikota Quartzite (Nagaraja Rao *et al.* 1987). In Chitravati Group, the basal sedimentary unit is thin persistent bed of conglomerate with jasper/oolitic chert, quartz, and quartzite, which is traversed by quartz veins. The east–west trending thin persistent (~50 m) Pulivendla Quartzite (1923 ± 22 Ma; Collins *et al.* 2015) starts with a chert pebble conglomerate and quartzite sequence. It is exposed mainly at Thallapalli ($14^{\circ}22'38.8''N$, $78^{\circ}23'36.7''E$), Rajupalem ($14^{\circ}26'20.7''N$, $78^{\circ}29'30.9''E$) areas on eastern side and Lingala ($14^{\circ}30'01.0''N$, $78^{\circ}06'21.3''E$), Velidandla ($14^{\circ}32'46.0''N$, $78^{\circ}03'13.5''E$) areas on the northwest side of Pulivendla town with gentle dip along the NE–SW strike. In the Mustukota ($14^{\circ}50'34.9''N$, $77^{\circ}52'23.9''E$) area, the quartzites are exposed with symmetrical ripple marks (figure 3a).

The Pulivendla Quartzite is overlain by the thick Tadpatri Formation, which is comprised of shale, ash fall felsic tuffs (1862 ± 9 Ma; Sheppard *et al.* 2017a), intrusives (1885 ± 3 Ma; French *et al.* 2008; 1899 ± 20 Ma; Anand *et al.* 2003); quartzite and dolomite. Gandikota Quartzite (1181 ± 29 Ma;

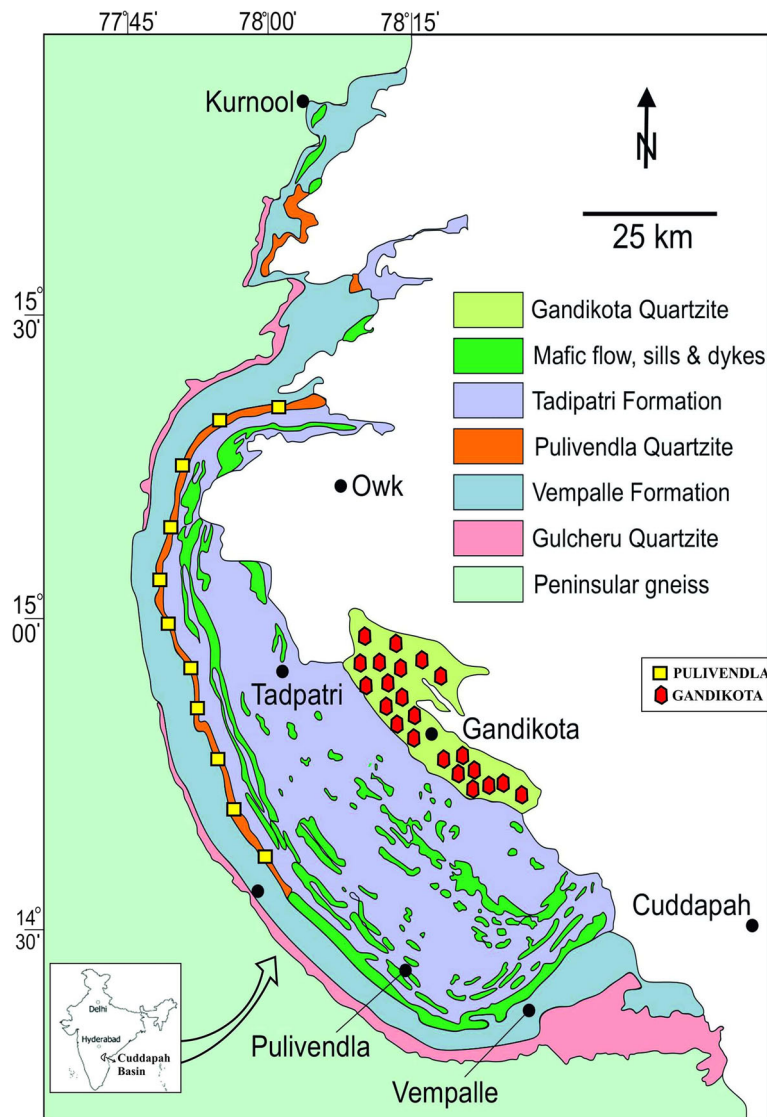


Figure 1. Generalised geological map of Papaghni sub-basin showing various formations of Papaghni and Chitravati Groups. Sample locations are marked (modified after Saha and Tripathy 2012).

Collins *et al.* 2015) is the topmost formation of the Chitravati Group, which has gradational contact with Tadpatri shale (Nagaraja Rao *et al.* 1987; Lakshminarayana *et al.* 2001). The sandstone–shale intercalations and medium to coarse grained quartz-arenite to feldspathic arenite represent the Gandikota Quartzite. It is geographically distributed mainly in the Gandikota hill range (14° 47'55.8"N, 78° 17'00.3"E), Muddanuru to Jammalamadugu road section and Nossam (14° 58' 15.0"N, 78° 22'40.6"E), Kanakadri Palli (15° 02' 45.3"N, 78° 03'57.8"E) areas as inliers (Nagaraja Rao *et al.* 1987; Reddy *et al.* 1990). The nature of the beds in the Gandikota formation shows gentle (10–15°) dip with the outcrop pattern giving rise to a synclinal structure termed as

Nawabpur syncline (Nagaraja Rao 1974). Herringbone cross bedding and ripple marks are the major primary sedimentary structures observed in these quartzites (figure 3b). Mainly two members of lithofacies of Gandikota Formation signify prograding shoreline depositional setting, a tide dominated shallow marine environment respectively (Lakshminarayana and Bhattacharjee 2000). Primary sedimentary structures, predominantly ripple marks are common in both Pulivendla and Gandikota formations (figure 3a and c). Six phases of contemporaneous igneous activity were reported in the form of basic sills, flows, ash fall tuffs and volcanic flows within Papaghni sub-basin (Sen and Narasimha Rao 1967; Sai 2014).

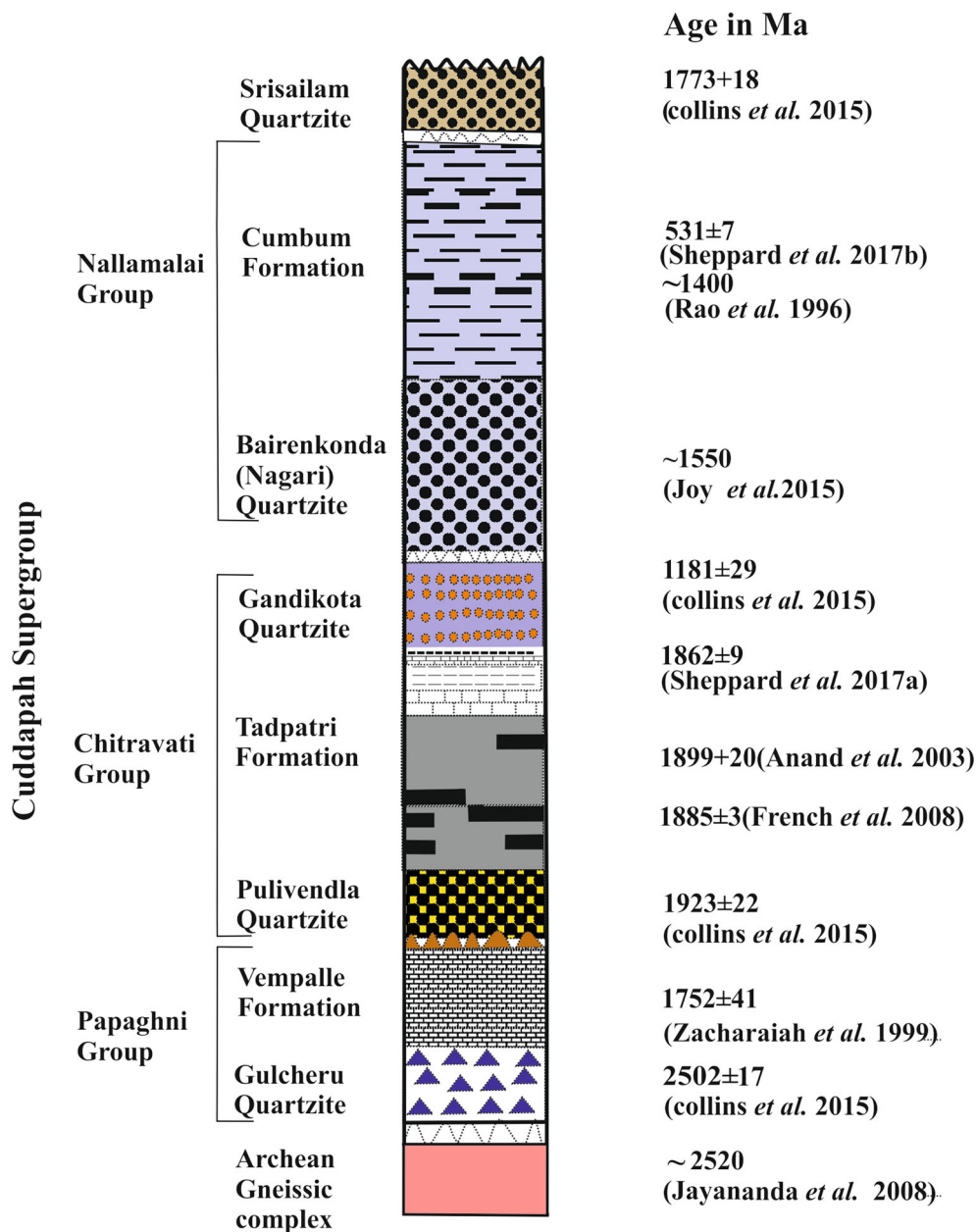


Figure 2. Stratigraphic lithology (not to scale) of Cuddapah Supergroup (after Nagaraja Rao *et al.* 1987; Anand *et al.* 2003).

Nallamalalai Group is composed of lower Bairenkonda Quartzite (Nagari), and upper Cumbum (Pullampet shale) Formation (Nagaraja Rao *et al.* 1987; Saha and Tripathy 2012). The Nallamalalai Group is thrust over the lowest Papaghni, Chitravati groups and the uppermost Srisailam Formation and Kurnool Group of the Cuddapah Basin (Saha and Chakraborty 2003; Saha *et al.* 2010; Collins *et al.* 2015) along Rudravaram line (Saha *et al.* 2010) or major Maidukuru thrust (Meijerink *et al.* 1984; Patranabis-Deb *et al.* 2012). The Nallamalalai Group consists of the lower

Bairenkonda (Nagari) Formation, which is sandstone dominated and the upper Cumbum (Pullampeta) Formation consisting mainly of shales punctuated by sandstones and dolomites. The basal part of the Bairenkonda Formation was deposited between 1659 and 1590 Ma (Joy *et al.* 2015). The youngest age limit of the Nallamalalai Group was constrained to be as ~1400 Ma old, which is in the form of Chelima lamproite (intrusion in to the Cumbum Formation; Rao *et al.* 1996, 1999, 2012; Kumar *et al.* 2001). Pan-African overprint of 531 Ma was recently confirmed by dating

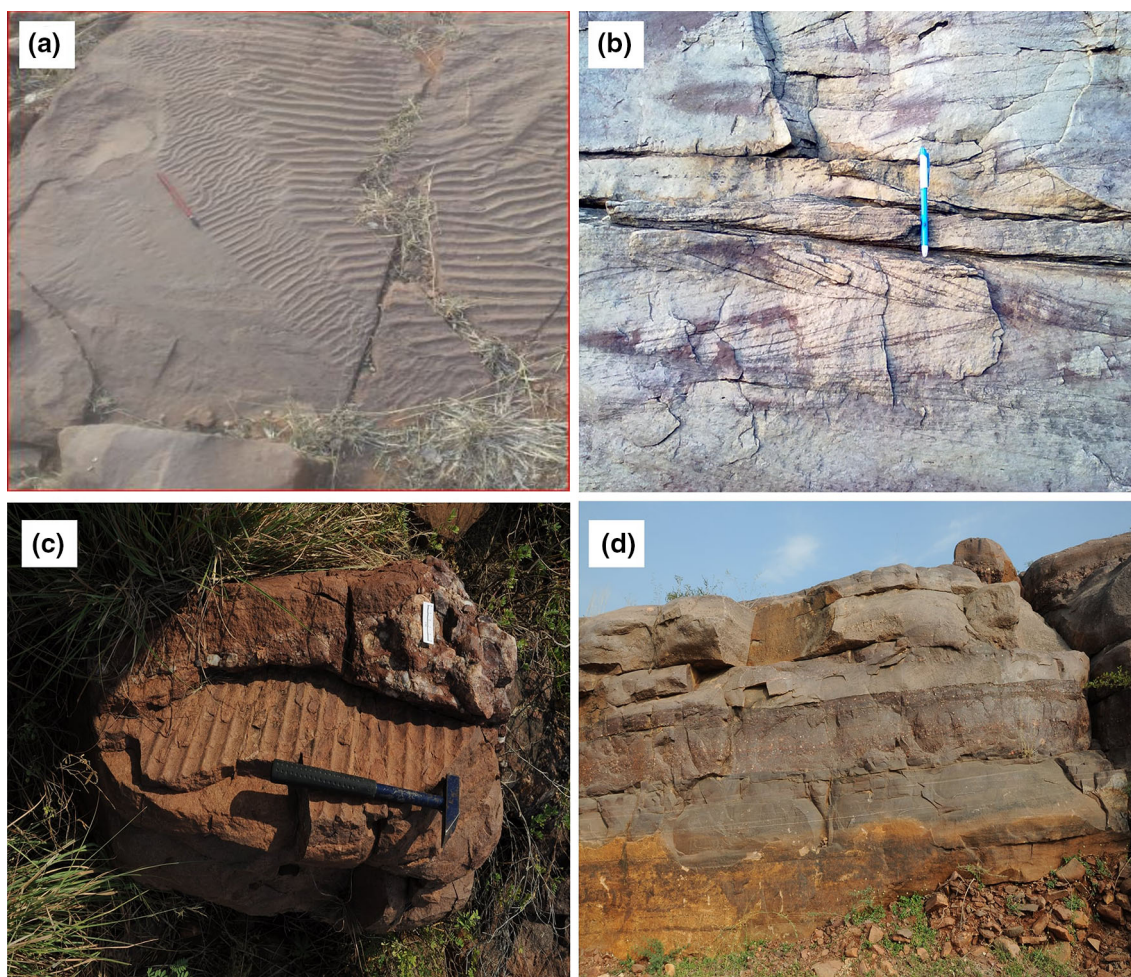


Figure 3. Field photographs of Pulivendla and Gandikota Quartzite. (a) Ripple marks on Pulivendla Quartzite together symmetric and asymmetric ripples are present. (b) Herring bone crossbedding of Gandikota Quartzite. (c) Symmetrical ripples on Pulivendla Quartzite with Chert pebbles. (d) Graded bedding nature of massive quartzite with facies variations.

monazite from low grade metamorphic black shales from Cumbum Formation at Mangampet barite mine region (Sheppard *et al.* 2017b).

3. Sampling and analytical techniques

For the purpose of petrography and geochemical studies, 41 representative samples of quartzites from Pulivendla and Gandikota formations of Chitravati Group were collected. At the time of sampling, care has been taken to select fresh rock samples. Thin sections for petrographic studies were prepared at Geochemistry Division, CSIR-National Geophysical Research Institute.

Major elements have been analyzed by X-ray Fluorescence (XRF) spectrometer (Axios, PANalytical) and trace elements have been analyzed using high resolution inductively coupled plasma mass spectrometer (HR-ICP-MS; Nu

Instruments Attom, UK) at CSIR-National Geophysical Research Institute, Hyderabad. The precision, accuracy and the analytical protocols of the data are given by Krishna *et al.* (2007) and Satyanarayanan *et al.* (2014) for XRF and HR-ICP-MS, respectively.

4. Petrography

4.1 Pulivendla Quartzite

The Pulivendla Quartzite contains quartz as the main mineral, which is in detrital mode in the form of common quartz (monocrystalline quartz), polycrystalline quartz (recrystallised quartz and stretched metamorphic quartz; figure 4a) followed by feldspar in the form of K-feldspar (orthoclase and microcline) and plagioclase (figure 4f). Sericitization is observed in some sections. Mica is present in the form of biotite and muscovite. The rock

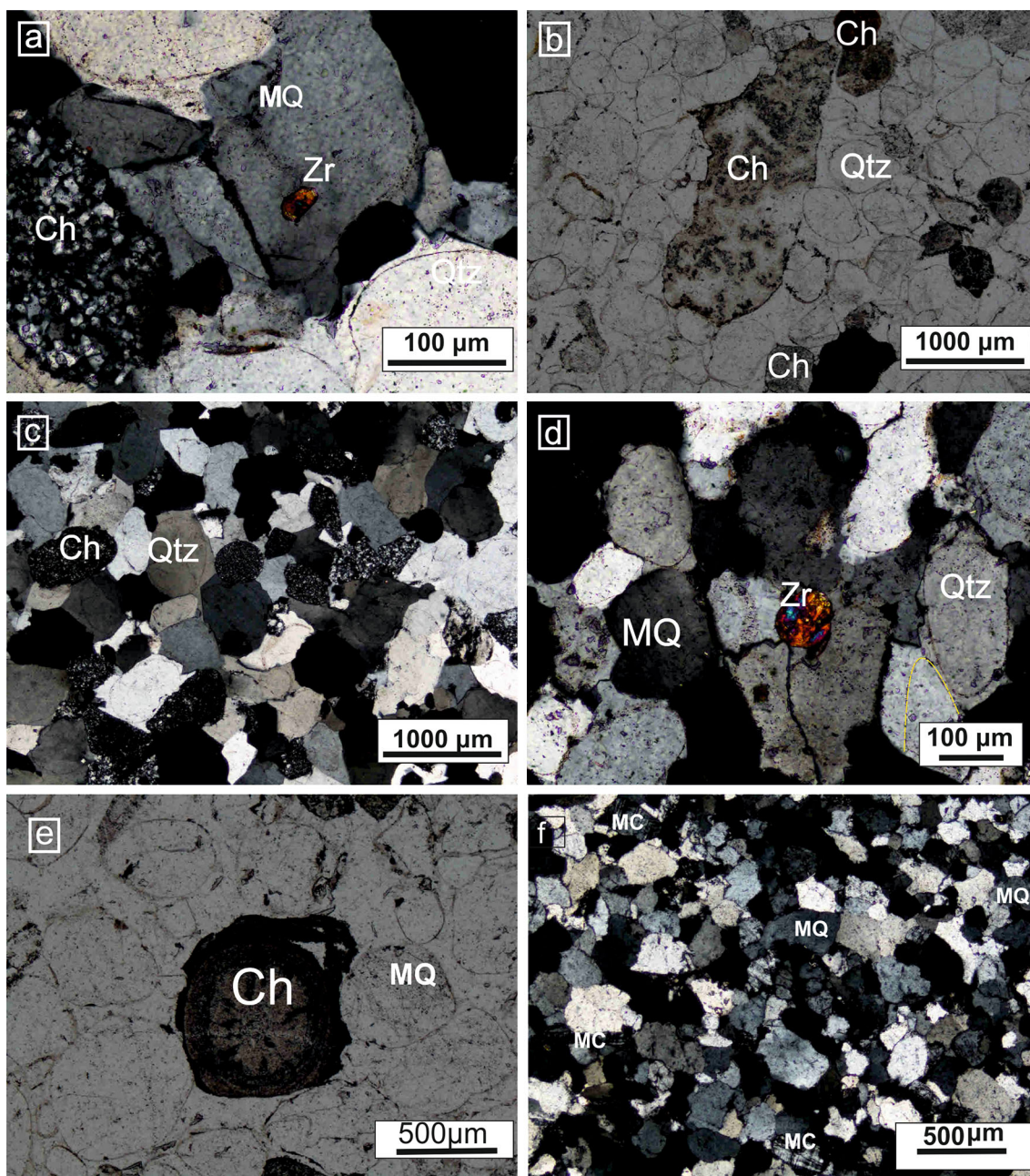


Figure 4. Microphotographs of Pulivendla Quartzite. (a) Pulivendla Quartzite showing monocrySTALLINE well-rounded quartz (Qtz) with over growth, detrital Zircon grain (Zr) overlapping on monocrySTALLINE quartz grain. Well-rounded quartz grains are replaced by chert grains (Ch). Moderate to well-rounded chert clasts in the form of cryptocrystalline to microcrystalline can be seen in the photomicrograph. (b) Elongated chert grain encircled by overgrowth quartz grains. Opaque minerals are showing dark colour (ppl). (c) Majority of well-rounded to subrounded chert grains surrounded by overgrowth quartz grains, quartz grains replaced by chert grains (Ch). (d) Well-rounded detrital Zircon enclosed by well-sorted monocrySTALLINE quartz grains. (e) This photograph shows ooids with well-developed radial and concentric structures encircled by well-rounded quartz grains. (f) Pulivendla Quartzite showing subangular grains and are well sorted.

fragments (siliceous oolites) and heavy minerals (zircon, apatite) are also present (figure 4d). The quartz grains are mainly fine to medium grained, well sorted and also contain subrounded to well-rounded grains (figure 4d) with secondary overgrowths (forming a quartz cement; figure 4b)

in optical continuity with the clasts. The main cementing material is silica with lesser amount of carbonate. The resulting new grains (clasts plus their overgrowths) form a roughly polygonal aggregate. Some of the grain contacts are irregular to sutured (figure 4c). Chert grains showing

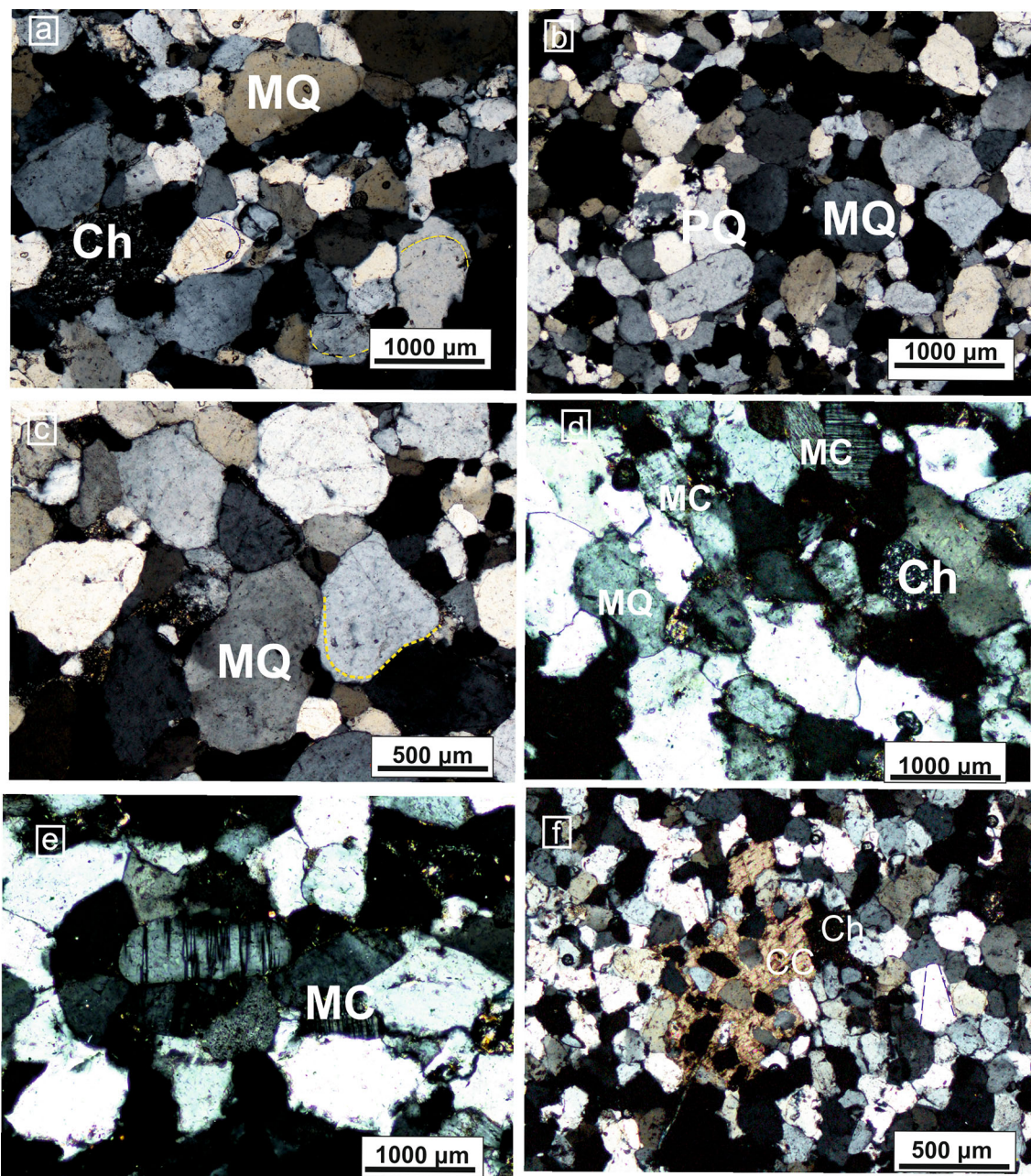


Figure 5. Microphotographs of Gandikota Quartzite. (a) Subangular grains of feldspar and quartz are well sorted. Secondary overgrowth of silica (in optical continuity). A common feature of diagenesis (Xed) discontinuous lines showing original grain boundaries and silica overgrowth. (b) Quartz is the dominant framework grain; it is in the form of monocrystalline quartz (MQ), lesser content of polycrystalline quartz (PQ). Silica is the main cementing material. Monocrystalline quartz predominates over polycrystalline type. (c) Quartz grains showing concave contact at centre. An authigenic overgrowth on a detrital quartz grain arrow mark showing. Monocrystalline quartz (MQ) is common. (d) Angular feldspar grains with chert and opaque minerals. Fresh and unaltered microcline showing typical cross hatched (Tartan) twinning under Xed nicols. Chert (Ch) replaced the subrounded quartz grain. (e) Microcline and feldspar with opaque minerals. (f) Carbonate cementing (CC) material at centre of photograph with subangular to rounded quartz grains. Overgrowth of quartz grains showing optical continuity.

oolitic (silicious) texture and are surrounded by well rounded quartz grains (figure 4e). Subangular to angular with well sorted quartz grains and microcline grains reflecting the textural immaturity of sediments (figure 4f).

Modal analysis of the Pulivendla Quartzite using point counting method reflecting the average quartz percentage in the form of monocrystalline and polycrystalline grains is about 92%, feldspar along with plagioclase and microcline is 4%, lithic

fragments (including chert) and matrix is 1%. Based on Qt–F–L ternary diagram (Dickinson 1985; figure 6a), the Pulivendla Quartzite is plotted in the craton interior and recycled orogenic fields. Subsequently, the sandstone classification triangular diagram (Folk 1974; figure 6b) represents the Pulivendla Quartzite which are in the fields of sub-arkose, quartz-arenite, sub-litharenite.

4.2 Gandikota Quartzite

Gandikota Quartzite contains quartz as the main detrital mode in the form of common quartz with undulose extinction (monocrystalline), polycrystalline quartz (figure 5a and b) followed by K-feldspar (orthoclase and microcline) and plagioclase (figure 5d). Silica cement occurs in the form of overgrowth around quartz detrital grains (figure 5c). Mica is present in the form of muscovite and biotite. The thin sections of the Gandikota Quartzite show absence of rock fragments. K-feldspar is common and it is altered to sericite. Common cementing material is silica, calcite is also observed in some sections (figure 5f). Chlorite and sericite occur as the main matrix material. Heavy minerals like zircon are present in euhedral shape and in the form of inclusions in quartz grains as they are mostly of detrital origin.

Modal analysis of Gandikota Quartzite using the point counting method average quartz including monocrystalline and polycrystalline quartz is 86%, feldspar including plagioclase and microcline is 6% and the rock fragments (chert) are 6%. In the Qt–F–L ternary diagram, these samples plot in craton interior field and recycled orogenic field (Dickinson 1985; figure 6a). Further using the modal analysis for sandstone classification triangular diagram (Folk 1974; figure 6b), Gandikota Quartzite plot in the quartz-arenite, sub-arkose, and sub-litharenite field.

5. Results

5.1 Major oxides

Pulivendla Quartzite contains higher content of SiO₂ (85.57–96.67, avg. 89.73) followed by lower proportion of Al₂O₃ (0.49–8.19, avg. 6.87), TiO₂ (0.01–0.17, avg. 0.04), Fe₂O₃ (0.01–1.94, avg. 0.47), MgO (0.01–0.47, avg. 0.15), CaO (0.04–0.14, avg. 0.09), Na₂O (0.02–1.31, avg. 0.09), K₂O (0.45–3.77, avg. 1.79) and P₂O₅ (0.00–0.14, avg. 0.02;

table 1). Gandikota Quartzites are also enriched in SiO₂ (79.94–89.34, avg. 86.80) with lower contents of Al₂O₃ (7.87–10.16, avg. 8.15), TiO₂ (0.00–0.24, avg. 0.06), Fe₂O₃ (0.01–5.36, avg. 0.89), MgO (0.01–2.60, avg. 0.36), CaO (0.04–0.45, avg. 0.10), Na₂O (0.02–1.11, avg. 0.42), K₂O (1.58–4.24, avg. 2.38) and P₂O₅ (0.0–0.06, avg. 0.02; table 2). On the basis of SiO₂ content, it has been suggested that the samples of the Pulivendla and Gandikota formations are quartz-rich to quartz-arenite type with the SiO₂ content ranging from 76 to 95% (Condie 1993). The lower content of CaO and Na₂O (< 1%) is consistent with the lower proportion of the plagioclase. The SiO₂/Al₂O₃ is >10, which indicates that sediments are highly mature. The K₂O/Na₂O ratio is ≫1 in both these quartzites, which is consistent with the petrographic observations that the K-feldspar dominates over plagioclase feldspar. In the geochemical classification diagram proposed by Pettijohn *et al.* (1987), quartzite samples of Pulivendla and Gandikota plotted in the fields of arkose to sub-arkose, sub-litharenite to quartz arenite (figure 7a).

5.2 Trace element geochemistry

The chondrite normalised REE patterns of Pulivendla and Gandikota quartzites are characterized by LREE enriched with La_N/Sm_N ratios varying from 1.33 to 5.48 (avg. 3.23) and 1.05 to 6.91 (avg. 3.81), respectively. Both quartzites of Pulivendla and Gandikota are characterized by flat to slightly concave upward HREE patterns with Gd_N/Yb_N ratio varying from 0.47 to 1.87 (avg. 1.09) for Pulivendla and 0.46 to 2.16 (avg. 1.30) for Gandikota Quartzite with negative Eu (Pulivendla = avg. 0.15, Gandikota = avg. 0.61) anomaly. On the basis of the REE patterns and their La_N/Yb_N ratio, the Pulivendla quartzites have been divided into two groups. The first group samples are showing low LREE and high HREE, while second group is of quartzite is characterized by high LREE and low HREE. The enrichment of HREE in the first group of samples is attributed to the presence of zircon in the samples. Zircon preferentially incorporate HREE relative to LREE resulting in fractionated REE pattern with low La_N/Yb_N ratios. The Zr and Hf also show a good correlation with HREE which also shows that zircon is a source of REE. Second group of samples is characterised by high LREE and low HREE, which is due to the quartz dilution effect. The quartz dilution effect is also supported by having

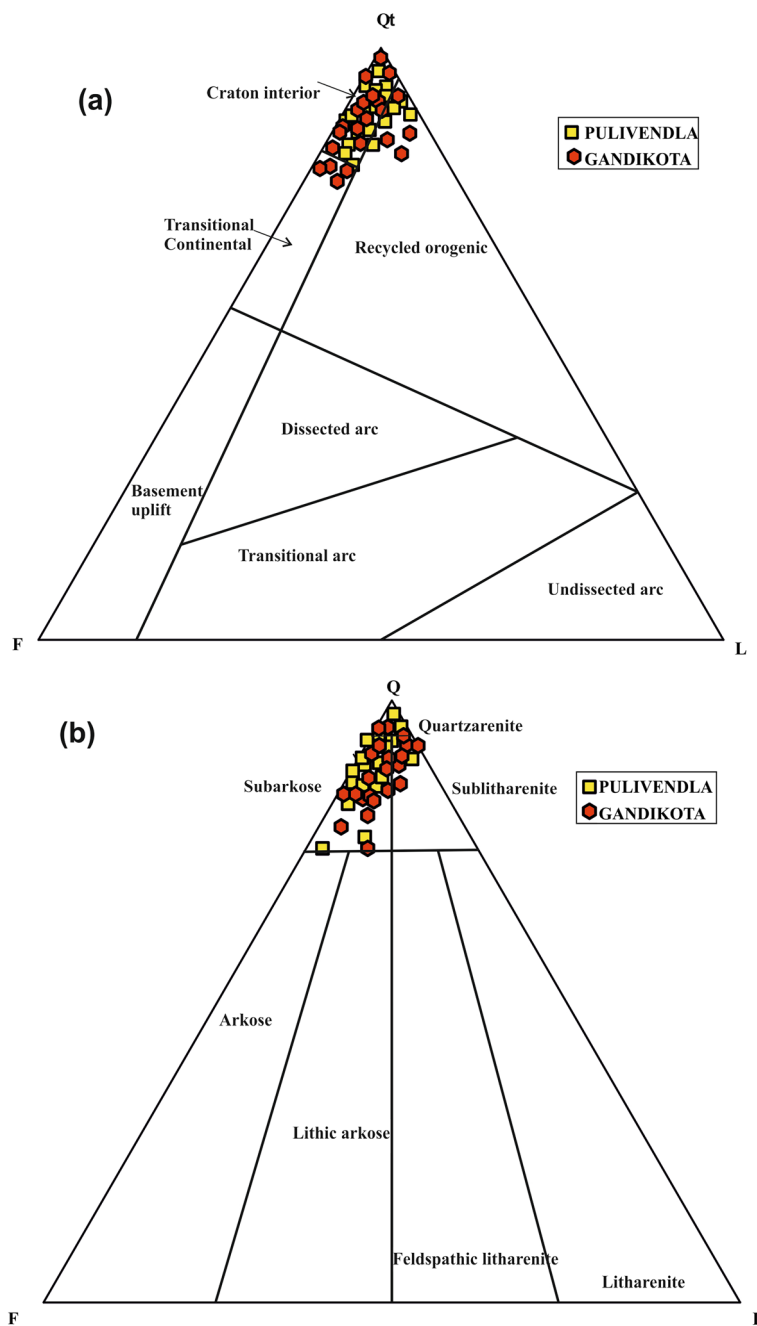


Figure 6. (a) Qt–F–L provenance ternary plot (after Dickinson 1985) of Pulivendla and Gandikota Quartzite. (b) QFL ternary diagram of quartzites (after Folk 1974).

low Σ REE values as compared to the first group of quartzite (table 1). This indicates that samples of these formations were mainly derived from an old upper continental crust composed chiefly of felsic and intermediate source components (figure 8a and b).

The transition trace elements like Sc, V, Cr, Co and Ni also shows variable proportions in Pulivendla and Gandikota Quartzite. The quartzites of Pulivendla contain lower concentration of

Sc (0.43–2.67, avg. 1.14), Cr (2.07–34.79, avg. 9.38) and Ni (2.64–27.34, avg. 7.91) with overlying Gandikota Quartzite (Sc = 0.55–4.46, avg. 1.46; Cr = 2.16–36.88, avg. 9.84; Ni = 3.76–22.06, avg. 9.81) and average higher content of V (3.19–20.75, avg. 11.25) than Gandikota Quartzite (V = 2.11–34.09, avg. 9.56; tables 1 and 2). Transition trace elements are highly enriched in clay minerals during weathering processes. There is a positive correlation of Al_2O_3 with Cr ($r = 0.13$) and Ni ($r = 0.20$)

Table 1. Major and trace element concentrations of Pulivendla Quartzites. Major oxides in wt%, trace and REEs in ppm. Normalising values of *McDonough and Sun (1995)*.

	PQ-14	PQ-15	PQ-23	PQ-58	PQ-59	PQ-11	PQ-20	PQ-21	PQ-22	PQ-23	PQ-27
SiO ₂	85.57	86.15	86.52	96.67	96.47	89.34	89.42	89.64	88.64	89.49	89.29
Al ₂ O ₃	7.98	7.95	8.19	1.10	1.94	7.87	7.88	7.89	7.99	7.90	7.99
Fe ₂ O ₃	0.39	0.43	0.23	0.88	0.49	0.02	0.01	0.01	0.65	0.20	0.18
MnO	0.00	0.00	0.00	0.02	0.01	0.01	0.00	0.00	0.00	0.00	0.00
MgO	0.01	0.02	0.02	0.15	0.12	0.40	0.09	0.10	0.47	0.09	0.11
CaO	0.07	0.05	0.04	0.05	0.04	0.12	0.10	0.10	0.13	0.09	0.09
Na ₂ O	1.31	1.12	1.10	0.05	0.05	0.02	0.03	0.05	0.02	0.03	0.02
K ₂ O	3.77	3.66	3.18	0.62	0.45	1.77	1.65	1.66	1.59	1.61	1.65
TiO ₂	0.03	0.06	0.01	0.04	0.04	0.02	0.17	0.09	0.01	0.02	0.01
P ₂ O ₅	0.02	0.03	0.02	0.03	0.03	0.02	0.01	0.01	0.02	0.01	0.01
LOI	0.86	0.53	0.68	0.40	0.36	0.41	0.65	0.45	0.48	0.57	0.65
CIA	55.65	57.40	60.59	56.58	75.13	78.45	79.64	79.25	80.04	80.13	80.11
PIA	63.13	67.28	71.59	71.24	90.36	95.98	96.35	95.83	95.87	96.67	96.91
ICV	0.84	0.79	0.68	1.70	0.68	0.41	0.31	0.31	0.45	0.30	0.30
CIW	77.81	80.39	81.31	86.40	92.60	96.93	97.15	96.75	96.74	97.38	97.58
K ₂ O/Na ₂ O	2.89	3.25	2.89	12.40	9.00	89.00	55.00	33.20	79.50	54.00	82.00
K ₂ O/Al ₂ O ₃	0.16	0.14	0.13	0.05	0.23	0.00	0.00	0.01	0.00	0.00	0.00
Al ₂ O ₃ /TiO ₂	268.67	134.33	826.00	27.50	48.5	396.50	46.41	87.44	798.00	396.50	794.00
Sc	1.00	0.77	0.81	1.93	2.67	0.69	1.83	1.99	0.68	0.96	0.78
V	14.02	11.53	12.84	10.03	20.75	5.86	11.04	12.72	8.77	8.86	8.34
Cr	34.79	25.07	27.11	7.20	7.93	2.25	2.87	4.82	7.04	4.49	7.94
Co	186.86	204.27	234.97	191.54	188.33	1.08	0.96	1.42	4.36	1.14	2.58
Ni	18.29	21.08	27.34	2.64	8.13	3.54	3.86	4.81	6.27	4.75	5.87
Ga	16.07	28.43	9.63	0.40	1.08	1.03	1.35	1.45	0.90	0.90	1.04
Rb	40.68	80.79	20.78	18.01	33.26	10.61	6.24	7.26	3.86	2.88	7.27
Sr	2.85	1.94	0.69	1.81	1.71	6.00	2.20	4.31	3.73	2.20	5.60
Y	41.33	34.16	7.13	14.39	14.40	2.61	60.17	31.96	2.00	5.15	3.41
Zr	20.78	29.14	11.78	23.22	44.04	87.17	70.77	197.22	62.49	107.96	91.84
Nb	1.89	3.45	4.99	22.15	49.44	1.91	3.82	3.64	3.18	1.35	1.22
Ba	83.13	9.46	78.32	34.75	30.41	1127.62	100.95	127.73	39.03	107.77	66.39
Hf	2.60	0.54	2.67	1.16	0.99	1.20	0.92	2.98	1.02	1.59	1.28
Th	0.74	1.07	3.13	6.76	2.59	2.53	3.18	6.96	2.71	2.52	2.56
U	0.28	0.61	0.74	1.90	2.20	0.45	1.12	2.37	0.80	0.71	0.58
La	3.43	9.93	3.74	9.90	30.55	2.70	7.70	4.52	1.26	0.76	4.86
Ce	6.26	20.76	6.12	15.81	57.61	6.39	16.53	12.02	3.51	2.09	13.18
Pr	0.77	2.32	0.83	2.26	7.04	0.74	2.23	1.59	0.42	0.25	1.53
Nd	2.71	8.01	2.95	9.61	28.77	2.76	10.21	7.17	1.60	1.01	5.64
Sm	0.44	1.13	0.56	1.91	5.48	0.42	3.01	2.02	0.32	0.28	0.95
Eu	0.11	0.24	0.15	0.40	0.96	0.10	1.07	0.40	0.06	0.08	0.11
Gd	0.42	0.85	0.65	1.83	5.38	0.42	4.77	2.74	0.33	0.41	0.88
Tb	0.06	0.12	0.12	0.36	0.95	0.07	1.26	0.67	0.06	0.11	0.14
Dy	0.33	0.58	0.70	2.70	6.62	0.49	11.11	5.65	0.38	0.93	0.77
Ho	0.07	0.12	0.15	0.33	0.79	0.12	2.64	1.39	0.09	0.23	0.17
Er	0.19	0.36	0.43	1.12	2.59	0.36	7.71	4.19	0.26	0.69	0.44
Tm	0.03	0.06	0.07	0.15	0.31	0.05	1.02	0.56	0.04	0.09	0.06
Yb	0.22	0.41	0.47	1.49	3.11	0.38	7.39	4.09	0.27	0.71	0.38
Lu	0.04	0.07	0.08	0.26	0.50	0.06	1.16	0.65	0.04	0.11	0.06
ΣREE	15.08	44.96	17.02	48.11	150.65	15.06	77.82	47.65	8.65	7.77	29.16
La/Sc	3.43	12.83	4.65	5.12	11.43	3.94	4.21	2.27	1.86	0.79	6.23
Th/Sc	0.74	1.38	3.89	3.50	0.97	3.70	1.73	3.49	3.99	2.62	3.28
Cr/Th	47.05	23.39	8.65	1.07	3.06	0.89	0.90	0.69	2.60	1.78	3.11

Table 1. (Continued.)

	PQ-14	PQ-15	PQ-23	PQ-58	PQ-59	PQ-11	PQ-20	PQ-21	PQ-22	PQ-23	PQ-27
Co/Th	252.7	190.55	74.96	28.34	72.68	0.43	0.30	0.20	1.61	0.45	1.01
(La/Yb) _N	10.55	16.63	5.45	4.51	6.67	4.87	0.71	0.75	3.12	0.73	8.73
(La/Sm) _N	4.84	5.48	4.18	3.24	3.48	3.99	1.60	1.39	2.43	1.70	3.18
(Gd/Yb) _N	1.54	1.70	1.14	0.99	1.40	0.89	0.52	0.54	0.97	0.47	1.87
Eu/Eu*	0.20	0.18	0.19	0.16	0.13	0.18	0.21	0.13	0.14	0.18	0.09
	PQ-28	PQ-29	PQ-30	PQ-32	PQ-33	PQ-34	PQ-47	PQ-48	Avg.	Min.	Max.
SiO ₂	88.95	89.03	88.82	89.04	94.46	89.06	89.06	89.36	89.73	85.57	96.67
Al ₂ O ₃	7.83	7.84	7.86	7.97	1.94	7.94	7.88	7.98	6.94	1.09	8.19
Fe ₂ O ₃	0.37	0.37	0.75	0.56	0.96	0.60	0.22	0.18	0.39	0.01	0.95
MnO	0.00	0.00	0.00	0.00	0.01	0.00	0.00	0.00	0.00	0.00	0.02
MgO	0.26	0.12	0.16	0.09	0.03	0.21	0.20	0.18	0.15	0.01	0.47
CaO	0.11	0.09	0.10	0.09	0.14	0.10	0.09	0.09	0.09	0.04	0.14
Na ₂ O	0.02	0.02	0.02	0.02	1.04	0.02	0.02	0.02	0.26	0.02	1.31
K ₂ O	1.69	1.70	1.76	1.61	0.70	1.66	1.65	1.67	1.79	0.45	3.77
TiO ₂	0.02	0.04	0.04	0.01	0.02	0.05	0.02	0.02	0.04	0.01	0.17
P ₂ O ₅	0.01	0.00	0.01	0.01	0.14	0.01	0.01	0.01	0.02	0.00	0.14
LOI	0.75	0.80	0.49	0.60	0.57	0.35	0.85	0.48	0.58	0.35	0.86
CIA	79.15	79.40	78.74	80.41	41.73	79.83	79.91	79.89	72.73	41.73	80.41
PIA	96.28	96.85	96.55	96.94	37.74	96.62	96.89	96.89	87.15	37.73	96.93
ICV	0.38	0.33	0.39	0.32	1.77	0.38	0.34	0.33	0.57	0.29	1.76
CIW	97.13	97.57	97.36	97.59	49.85	97.36	97.58	97.58	91.24	49.84	97.59
K ₂ O/Na ₂ O	85.00	85.50	89.00	80.50	0.68	82.50	83.00	83.00	53.28	0.68	89.00
K ₂ O/Al ₂ O ₃	0.00	0.00	0.00	0.00	0.53	0.00	0.00	0.00	0.27	0.19	0.56
Al ₂ O ₃ /TiO ₂	393.50	197.25	198.25	796.00	98.50	158.40	396.50	396.00	339.90	27.5	826.00
Sc	0.95	1.04	1.22	0.64	1.57	1.07	0.68	0.43	1.14	0.43	2.67
V	19.97	8.74	13.00	19.46	11.28	5.96	7.41	3.19	11.25	3.19	20.75
Cr	7.03	3.26	14.99	2.07	3.09	5.74	7.99	2.59	9.38	2.07	34.79
Co	1.98	0.81	4.12	1.16	1.42	2.26	1.99	0.86	54.32	0.81	234.97
Ni	7.39	4.21	8.79	3.45	4.06	5.62	6.18	4.10	7.91	2.64	27.34
Ga	0.92	0.87	1.54	0.52	2.08	0.98	0.98	0.34	3.71	0.34	28.43
Rb	9.84	9.56	13.71	2.97	19.90	7.79	9.61	2.01	16.16	2.01	80.79
Sr	27.92	1.61	28.26	5.88	20.50	3.62	4.00	17.78	7.50	0.69	28.26
Y	3.85	2.49	3.63	1.79	20.81	4.37	2.72	0.97	13.54	0.97	60.17
Zr	68.55	276.98	118.74	47.65	339.31	411.51	28.22	11.85	107.85	11.78	411.51
Nb	1.20	2.26	1.55	0.93	3.22	3.97	1.73	0.22	5.90	0.22	49.44
Ba	74.00	40.13	68.18	28.93	857.94	158.78	84.82	26.15	165.50	9.46	1127.62
Hf	0.98	4.03	1.60	0.76	4.96	5.72	0.33	0.13	1.87	0.13	5.72
Th	1.85	3.55	3.05	1.99	4.02	6.76	2.04	0.76	3.09	0.74	6.96
U	1.10	0.56	1.09	0.53	1.25	1.03	0.61	0.45	0.97	0.28	2.37
La	2.48	1.86	4.61	1.36	7.70	3.56	3.33	1.77	5.58	0.76	30.55
Ce	4.79	4.59	12.41	3.26	13.04	9.86	8.73	3.45	11.60	2.09	57.61
Pr	0.63	0.52	1.42	0.39	2.32	1.12	1.01	0.42	1.46	0.25	7.04
Nd	2.80	1.88	5.10	1.53	13.83	4.02	3.76	1.70	6.06	1.01	28.77
Sm	0.51	0.34	0.93	0.25	3.61	0.64	0.58	0.25	1.24	0.25	5.48
Eu	0.10	0.06	0.13	0.04	0.80	0.11	0.09	0.04	0.27	0.04	1.07
Gd	0.53	0.34	0.88	0.25	3.70	0.63	0.53	0.23	1.36	0.23	5.38
Tb	0.10	0.06	0.14	0.05	0.66	0.12	0.09	0.04	0.27	0.04	1.26
Dy	0.68	0.44	0.82	0.32	4.29	0.82	0.55	0.21	2.02	0.21	11.11
Ho	0.16	0.11	0.18	0.08	0.94	0.20	0.13	0.05	0.42	0.05	2.64
Er	0.47	0.35	0.47	0.24	2.50	0.62	0.39	0.13	1.24	0.13	7.71

Table 1. (Continued.)

	PQ-28	PQ-29	PQ-30	PQ-32	PQ-33	PQ-34	PQ-47	PQ-48	Avg.	Min.	Max.
Tm	0.06	0.05	0.06	0.03	0.31	0.09	0.05	0.02	0.16	0.02	1.02
Yb	0.43	0.43	0.43	0.26	2.20	0.69	0.40	0.12	1.26	0.12	7.39
Lu	0.06	0.07	0.06	0.04	0.33	0.12	0.06	0.02	0.20	0.02	1.16
Σ REE	13.79	11.11	27.64	8.10	56.24	22.59	19.70	8.44	33.13	7.77	150.65
La/Sc	2.60	1.79	3.77	2.14	4.91	3.33	4.92	4.09	4.44	0.79	12.83
Th/Sc	1.94	3.42	2.50	3.13	2.56	6.33	3.02	1.75	2.84	0.74	6.33
Cr/Th	3.79	0.92	4.91	1.04	0.77	0.85	3.91	3.42	5.94	0.69	47.05
Co/Th	1.07	0.23	1.35	0.59	0.35	0.33	0.97	1.14	33.12	0.20	252.7
(La/Yb) _N	3.96	2.97	7.34	3.52	2.38	3.51	5.67	9.80	5.36	0.71	16.63
(La/Sm) _N	3.04	3.46	3.11	3.44	1.33	3.48	3.61	4.42	3.23	1.33	5.48
(Gd/Yb) _N	1.00	0.64	1.66	0.77	1.36	0.75	1.08	1.51	1.09	0.47	1.87
Eu/Eu*	0.15	0.14	0.11	0.13	0.17	0.13	0.12	0.11	0.15	0.09	0.21

PQ = Pulivendla Quartzite, Avg. = average, Min. = Minimum, Max. = Maximum.

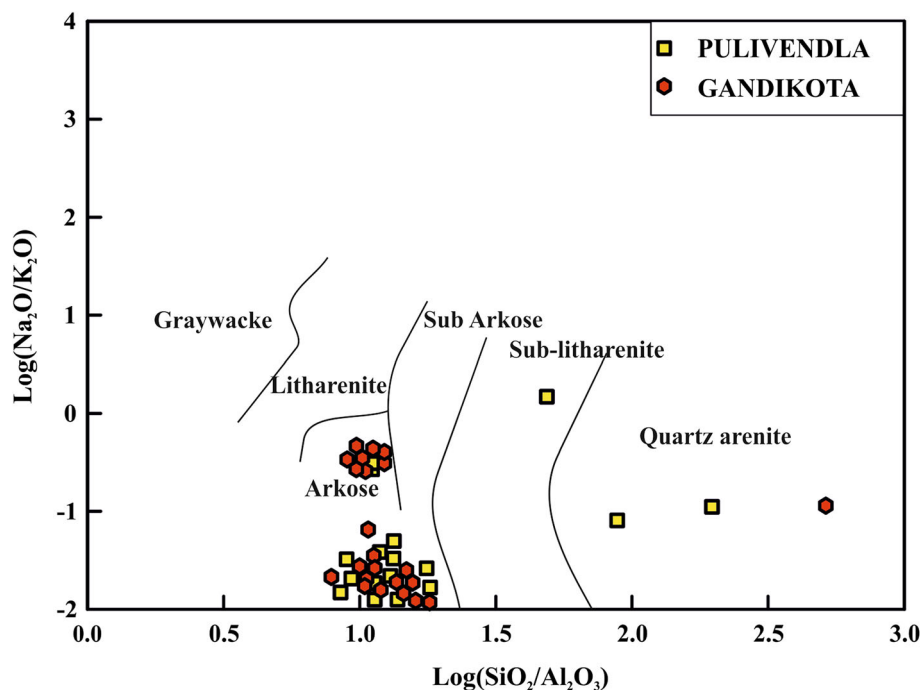


Figure 7. Sandstone classification diagram using $\log(\text{Na}_2\text{O}/\text{K}_2\text{O})$ vs. $\log(\text{SiO}_2/\text{Al}_2\text{O}_3)$ (after Pettijohn *et al.* 1987).

of Chitravati Quartzite with very small negative correlation in Sc ($r = -0.15$) and V ($r = -0.06$), which suggest that these elements are more or less controlled by aluminosilicate minerals and the nature of the source rocks. The positive correlation of the Ni with Fe_2O_3 ($r = 0.03$) suggest possible association of Ni with Fe-oxide minerals.

The large ion lithophile elements (LILEs) are present in variable proportions in these quartzites. The Pulivendla Quartzites are characterized by similar Rb (2.01–80.79, avg. 16.16) and lower content of Sr (0.69–28.26, avg. 7.50), Ba (9.46–1127.62, avg. 165.50), Th (0.74–6.96, avg. 3.09) and U (0.28–2.37, avg. 0.97) compared to Gandikota Quartzite,

Rb (1.16–91.06, avg. 11.54), Sr (2.32–260.61, avg. 43.36), Ba (4.72–1994.42, avg. 196.47), Th (1.03–20.57, avg. 4.90) and U (0.28–4.70, avg. 1.01; tables 1 and 2). In the potassium-rich minerals, like K-feldspar and biotite, Rb generally coexists with potassium, while Sr tends to enrich in Ca-bearing minerals (Dasch 1969). Relatively high values of Rb occur in Pulivendla Quartzite which again indicates dominance of K-feldspar bearing rocks in the source terrain. But in case of Gandikota Quartzite, they have higher proportion of Sr than Rb.

In terms of high field strength elements (HFSE), both the Pulivendla and Gandikota Quartzites contain low to high Zr (11.78–411.51, avg. 107.85,

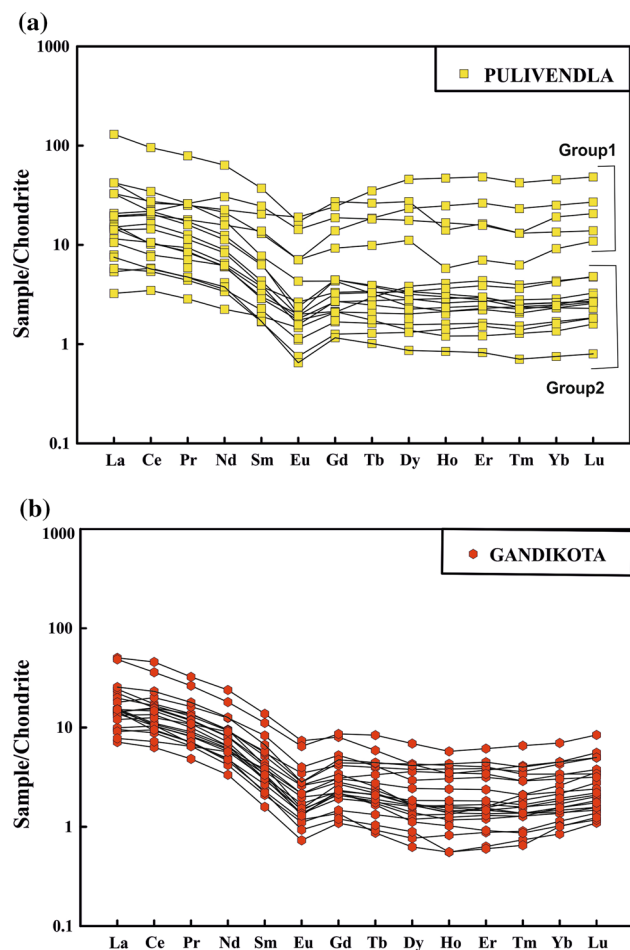


Figure 8. (a) Chondrite normalised REE pattern of Pulivendla Quartzite. (b) Chondrite normalised REE pattern of Gandikota Quartzite.

19.01–1243.97, avg. 291.29, respectively) and low to moderate Hf values (0.13–5.72, avg. 1.87, 0.66–25.50, avg. 5.87, respectively; tables 1 and 2).

6. Discussion

6.1 Source area weathering

Lithologies that show different degrees of weathering in different environments like warm and humid climate are susceptible to chemical weathering, whereas cold and dry climate are susceptible to mechanical weathering. The intensity and period of weathering in clastic sedimentary rocks can be estimated by examining the association between alkali and alkaline elements (Nesbitt and Young 1996; Nesbitt *et al.* 1997). Nesbitt and Young (1982), defined the Chemical Index of Alteration (CIA) formulae to calculate the amount of chemical weathering

$$CIA = \frac{[Al_2O_3 / (Al_2O_3 + CaO + Na_2O + K_2O)] \times 100. \quad (1)}$$

Oxides are in molar proportions and CaO represents the Ca in silicate fractions only. CIA values are of ~50 for unweathered igneous rocks to near 100 for residual clays (initial 50–60, intermediate 60–80 and extreme >80; Nesbitt and Young 1982; Fedo *et al.* 1995). The CIA values in the Pulivendla Quartzite range from 41–80 (avg. 72) and Gandikota Quartzite 60–80 (avg. 71), respectively (tables 1 and 2), suggestive of low to moderate chemical weathering in the source area.

The CIA values are also plotted in Al₂O₃–(CaO+Na₂O)–K₂O triangular plot (Nesbitt and Young 1984; Fedo *et al.* 1995; commonly referred as the ‘A–CN–K’ diagram) to categorize the provenance composition and weathering trends. The concept behind the use of this diagram is to understand the rate of weathering of plagioclase (Ca–Na feldspar) and K-feldspar (Middelburg *et al.* 1988). Thus, during weathering, CaO and Na₂O are preferentially leached relative to K₂O due to which the weathering trend moves parallel to the A–CN join. Intense weathering of a rock removes CaO, Na₂O and K₂O, making the trend parallel to the A–K join.

The studied samples of the Pulivendla and Gandikota Quartzite are plotted in the A–CN–K ternary diagram in which majority of the samples are plotted above the feldspar tie line and few samples at right of the five trend line towards K-feldspar, which suggest that these samples might have suffered minor amount of K-metasomatism. To ascertain the presence or absence of post-depositional K-metasomatism, we have carried out petrographic and geochemical assessment of each sample. The higher content of K₂O and Rb in few samples and sericitization of plagioclase is also suggestive of post-depositional K-metasomatism (figure 9a). On the basis of weathering trends of the studied samples, it has been suggested that samples have undergone moderate to intense chemical weathering, which could be due to either differential weathering conditions or that the least weathered samples are representative of source rock.

Some indices utilize major oxides to try and acquire more complete scenarios for chemical modification during weathering processes. Mafic Index of Alteration (MIA) expands the condition of the CIA to incorporate the significant components of

Table 2. Major and trace element concentrations of Gandikota Quartzites. Major oxides in wt%, trace and REEs in ppm. Normalising values of *McDonough and Sun (1995)*.

	GQ-8	GQ-9	GQ-10	GQ-11	GQ-12	GQ-13	GQ-24	GQ-25	GQ-35	GQ-36	GQ-37	GQ-38	GQ-39
SiO ₂	86.99	87.03	86.55	86.53	79.95	86.91	86.62	83.94	79.94	89.26	87.00	89.06	87.92
Al ₂ O ₃	8.35	8.25	8.22	8.03	8.22	7.91	8.25	8.18	10.16	7.94	8.21	7.98	7.91
Fe ₂ O ₃	0.06	0.01	0.01	0.14	5.36	0.01	0.01	2.51	1.90	0.01	0.60	0.02	1.77
MnO	0.00	0.00	0.00	0.00	0.03	0.00	0.00	0.00	0.02	0.00	0.00	0.00	0.00
MgO	0.02	0.01	0.02	0.01	0.01	0.01	0.01	0.02	2.60	0.12	0.43	0.12	0.08
CaO	0.06	0.04	0.05	0.04	0.08	0.04	0.04	0.09	0.14	0.09	0.11	0.09	0.09
Na ₂ O	1.11	1.11	1.11	1.10	1.09	1.09	1.10	1.11	0.09	0.02	0.05	0.02	0.02
K ₂ O	3.11	3.15	3.12	3.22	3.08	3.15	3.09	3.19	4.24	1.73	2.46	1.65	1.61
TiO ₂	0.00	0.02	0.01	0.08	0.10	0.07	0.02	0.18	0.24	0.04	0.12	0.03	0.03
P ₂ O ₅	0.03	0.02	0.02	0.03	0.03	0.03	0.02	0.03	0.02	0.01	0.02	0.01	0.02
LOI%	0.27	0.35	0.90	0.82	2.06	0.78	0.84	0.75	0.65	0.77	0.99	1.02	0.55
CIA	61.11	60.82	60.87	59.93	60.98	59.98	61.22	60.04	67.05	79.29	73.62	80.08	80.32
PIA	71.93	71.77	71.71	70.70	71.71	70.63	72.27	70.37	93.22	96.84	95.13	96.92	96.93
ICV	0.65	0.65	0.65	0.70	1.08	0.68	0.64	0.90	1.29	0.31	0.56	0.29	0.42
CIW	81.13	81.25	81.12	81.01	80.99	80.85	81.41	80.44	96.16	97.57	96.66	97.59	97.59
K ₂ O/Na ₂ O	2.79	2.83	2.81	2.93	2.83	2.87	2.80	2.88	8.75	46.78	86.00	48.80	82.50
K ₂ O/Al ₂ O ₃	0.37	0.38	0.38	0.40	0.37	0.40	0.37	0.39	1.84	0.42	0.22	0.30	0.21
Al ₂ O ₃ /TiO ₂	ND	415.00	831.00	101.25	84.70	114.57	419.50	45.83	6.33	42.04	197.00	68.00	265.67
Sc	0.66	0.84	0.76	1.53	2.34	1.71	0.55	2.97	4.46	0.74	1.58	0.66	0.69
V	9.24	10.23	7.57	7.95	18.93	4.88	3.72	11.76	34.09	3.92	8.70	4.44	18.43
Cr	19.06	21.58	17.66	14.48	36.88	12.23	14.22	14.79	5.93	2.16	2.37	2.88	2.96
Co	221.23	239.70	288.37	164.09	145.80	191.77	224.31	180.94	5.90	0.99	2.91	0.75	0.86
Ni	17.54	15.03	22.06	16.69	15.62	14.49	9.27	11.05	5.94	3.78	4.67	3.76	3.79
Ga	0.51	0.75	0.61	1.37	3.86	1.24	0.31	2.42	2.96	0.82	1.82	0.61	0.78
Rb	3.06	4.47	5.29	5.68	6.94	3.67	1.16	6.61	91.06	3.97	33.97	3.09	1.85
Sr	10.79	9.45	16.30	23.39	16.95	38.03	5.30	14.07	227.11	2.32	11.05	2.47	28.64
Y	2.22	2.21	1.89	2.11	5.44	2.03	0.87	8.74	4.41	1.38	3.98	0.91	0.99

Zr	70.46	57.28	65.31	235.53	491.4	394.07	80.57	827.37	1244.0	280.04	706.05	183.75	57.72
Nb	0.41	0.18	0.46	0.65	1.05	0.49	0.45	0.76	6.15	2.31	6.30	1.69	1.06
Ba	36.24	38.22	42.01	36.17	96.56	56.18	23.89	124.70	731.04	47.62	313.61	32.61	26.24
Hf	2.28	1.81	1.92	6.83	15.32	11.55	2.75	25.50	18.50	4.21	10.27	2.74	0.89
Th	1.03	1.58	1.05	8.73	4.44	12.07	1.83	5.89	20.57	4.66	9.61	4.02	2.28
U	0.28	0.63	0.36	0.71	1.80	0.62	0.29	1.69	4.70	0.71	1.05	0.41	0.32
La	3.24	5.22	3.48	5.72	11.83	3.63	3.43	11.43	4.66	2.25	4.22	1.68	2.33
Ce	6.29	9.52	6.48	10.42	27.60	6.66	5.61	21.72	10.02	5.32	12.07	3.80	6.26
Pr	0.72	1.21	0.77	1.22	2.88	0.81	0.63	2.35	1.15	0.58	1.45	0.43	0.73
Nd	2.59	4.30	2.79	4.24	10.80	2.93	2.08	8.16	4.21	1.89	5.64	1.51	2.72
Sm	0.45	0.61	0.44	0.76	2.02	0.53	0.34	1.63	0.82	0.31	1.22	0.23	0.50
Eu	0.10	0.12	0.08	0.15	0.41	0.11	0.07	0.36	0.19	0.06	0.22	0.04	0.08
Gd	0.45	0.56	0.41	0.67	1.58	0.43	0.27	1.70	0.82	0.29	1.03	0.21	0.43
Tb	0.08	0.08	0.07	0.09	0.21	0.06	0.03	0.30	0.14	0.05	0.15	0.03	0.06
Dy	0.40	0.42	0.34	0.40	1.03	0.32	0.15	1.67	0.92	0.29	0.71	0.19	0.27
Ho	0.08	0.08	0.07	0.08	0.19	0.07	0.03	0.32	0.21	0.07	0.17	0.05	0.06
Er	0.22	0.23	0.19	0.25	0.59	0.25	0.10	0.98	0.61	0.21	0.50	0.14	0.15
Tm	0.03	0.04	0.03	0.04	0.10	0.05	0.02	0.16	0.09	0.03	0.07	0.02	0.02
Yb	0.23	0.28	0.22	0.35	0.73	0.43	0.14	1.14	0.70	0.25	0.54	0.19	0.17
Lu	0.04	0.05	0.04	0.07	0.13	0.09	0.03	0.20	0.12	0.04	0.09	0.03	0.03
ΣREE	3.31	5.51	3.56	5.47	13.68	3.73	2.71	10.50	5.36	2.47	7.08	1.94	3.45
La/Sc	4.93	6.18	4.58	3.73	5.05	2.12	6.27	3.85	1.04	3.06	2.68	2.52	3.38
Th/Sc	1.56	1.88	1.38	5.69	1.90	7.06	3.35	1.98	4.61	6.34	6.09	6.05	3.30
Cr/Th	18.51	13.62	16.85	1.66	8.30	1.01	7.76	2.51	0.29	0.46	0.25	0.72	1.30
Co/Th	214.83	151.24	275.07	18.8	32.82	15.88	122.42	30.71	0.29	0.21	0.30	0.19	0.38
(La/Yb) _N	9.93	13.04	10.85	11.33	11.19	5.91	17.23	6.95	4.63	6.16	5.39	6.28	9.72
(La/Sm) _N	4.46	5.33	5.00	4.71	3.65	4.27	6.40	4.38	3.56	4.58	2.16	4.50	2.92
(Gd/Yb) _N	1.63	1.65	1.53	1.58	1.78	0.84	1.61	1.23	0.97	0.94	1.57	0.96	2.16
Eu/Eu*	0.65	0.63	0.61	0.63	0.70	0.71	0.67	0.66	0.72	0.63	0.60	0.56	0.53

Table 2. (Continued.)

	GQ-40	GQ-41	GQ-42	GQ-43	GQ-44	GQ-45	GQ-46	GQ-49	GQ-50	Avg.	Min.	Max.
SiO ₂	83.96	88.55	89.14	89.34	89.03	88.57	88.47	87.59	87.35	86.80	79.94	89.34
Al ₂ O ₃	8.05	7.88	7.99	8.01	7.91	8.00	7.92	7.87	8.13	8.15	7.87	10.16
Fe ₂ O ₃	3.70	0.91	0.04	0.01	0.80	0.47	0.57	0.48	0.11	0.89	0.01	5.36
MnO	0.01	0.00	0.01	0.00	0.00	0.00	0.01	0.00	0.00	0.00	0.00	0.03
MgO	1.27	0.08	0.08	0.08	0.08	0.28	0.35	1.04	1.22	0.36	0.01	2.60
CaO	0.45	0.09	0.09	0.09	0.09	0.11	0.15	0.13	0.12	0.10	0.04	0.45
Na ₂ O	0.03	0.02	0.02	0.02	0.02	0.02	0.02	0.03	0.14	0.42	0.02	1.11
K ₂ O	1.73	1.58	1.65	1.62	1.66	1.69	1.65	1.77	2.13	2.38	1.58	4.24
TiO ₂	0.02	0.03	0.06	0.03	0.06	0.04	0.04	0.10	0.05	0.06	0.00	0.24
P ₂ O ₅	0.01	0.00	0.01	0.00	0.01	0.06	0.04	0.02	0.02	0.02	0.00	0.06
LOI%	0.78	0.86	0.91	0.80	0.35	0.76	0.79	0.97	0.75	0.81	0.27	2.06
CIA	74.58	80.52	80.11	80.45	79.91	79.49	79.11	78.15	74.73	71.47	59.93	80.52
PIA	87.70	96.95	96.91	96.94	96.89	96.32	95.27	95.46	92.92	86.61	70.37	96.95
ICV	1.04	0.35	0.29	0.27	0.35	0.39	0.43	0.67	0.73	0.61	0.27	1.29
CIW	90.29	97.59	97.58	97.60	97.58	97.14	96.30	96.53	94.82	90.87	80.44	97.60
K ₂ O/Na ₂ O	81.00	58.00	80.00	82.00	80.50	83.00	83.50	83.00	59.67	44.83	2.79	86.00
K ₂ O/Al ₂ O ₃	0.20	0.22	0.20	0.21	0.20	0.21	0.21	0.21	0.23	0.36	0.20	1.84
Al ₂ O ₃ /TiO ₂	265.33	403.50	265.67	132.33	266.00	132.17	197.75	199	79.5	215.82	6.33	831.00
Sc	2.75	1.60	0.96	0.76	1.11	0.96	1.29	1.05	2.12	1.46	0.55	4.46
V	27.13	2.11	4.63	5.46	7.99	6.05	6.81	3.41	2.83	9.56	2.11	34.09
Cr	5.80	7.03	5.03	9.57	6.53	5.53	4.26	3.13	2.32	9.84	2.16	36.88
Co	1.90	143.47	1.51	2.35	1.14	2.13	2.01	3.13	2.32	83.07	0.75	288.37
Ni	6.89	15.74	6.06	7.77	5.08	6.53	5.11	9.80	9.24	9.81	3.76	22.06
Ga	1.29	0.64	0.76	0.90	1.01	1.22	0.96	1.18	2.46	1.30	0.31	3.86
Rb	15.78	8.93	2.92	4.84	4.19	8.31	7.78	12.53	17.69	11.54	1.16	91.06
Sr	260.61	24.74	3.40	6.57	5.22	15.52	6.36	93.61	132.00	43.36	2.32	260.61
Y	2.85	1.86	1.79	1.79	1.65	5.45	5.06	2.04	5.13	2.95	0.87	8.74
Zr	166.43	19.01	197.16	53.50	96.19	127.05	181.63	398.39	475.46	291.29	19.01	1243.97

Nb	1.88	0.60	2.26	1.03	1.89	2.00	2.44	2.57	2.32	1.77	0.18	6.30
Ba	1994.42	43.03	66.14	51.63	47.81	276.23	228.17	5.15	4.72	196.47	4.72	1994.42
Hf	2.35	0.66	2.47	0.81	1.33	1.92	2.40	5.71	6.95	5.87	0.66	25.50
Th	2.68	1.35	4.16	2.03	2.58	2.06	2.06	7.71	5.42	4.90	1.03	20.57
U	4.13	0.66	0.45	0.71	0.56	0.53	0.31	0.77	0.65	1.01	0.28	4.70
La	3.36	3.58	2.14	3.39	3.12	2.83	1.82	3.57	6.00	4.22	1.68	11.83
Ce	9.52	6.35	5.72	9.34	8.14	7.57	4.36	8.87	13.95	9.34	3.80	27.60
Pr	1.06	0.62	0.63	1.05	0.89	0.96	0.57	0.97	1.59	1.06	0.43	2.88
Nd	3.67	2.21	2.16	3.63	2.94	4.09	2.57	3.23	5.71	3.82	1.51	10.80
Sm	0.64	0.32	0.39	0.60	0.45	0.85	0.56	0.49	0.98	0.69	0.23	2.02
Eu	0.15	0.05	0.08	0.09	0.08	0.16	0.12	0.07	0.16	0.13	0.04	0.41
Gd	0.60	0.24	0.38	0.53	0.42	0.87	0.61	0.46	0.93	0.63	0.21	1.70
Tb	0.10	0.04	0.06	0.08	0.07	0.16	0.12	0.08	0.16	0.10	0.03	0.30
Dy	0.59	0.22	0.39	0.40	0.40	1.04	0.87	0.45	1.01	0.57	0.15	1.67
Ho	0.13	0.03	0.09	0.09	0.09	0.23	0.20	0.10	0.24	0.12	0.03	0.32
Er	0.38	0.10	0.27	0.24	0.23	0.64	0.54	0.29	0.71	0.36	0.10	0.98
Tm	0.05	0.01	0.04	0.03	0.03	0.08	0.07	0.04	0.10	0.05	0.01	0.16
Yb	0.37	0.16	0.30	0.24	0.25	0.55	0.49	0.31	0.73	0.40	0.14	1.14
Lu	0.06	0.03	0.05	0.04	0.04	0.08	0.08	0.05	0.12	0.07	0.03	0.20
ΣREE	4.74	2.83	2.79	4.68	3.83	5.06	3.14	4.20	7.30	4.88	1.94	13.68
La/Sc	1.22	2.23	2.23	4.46	2.81	2.95	1.41	7.36	2.56	3.48	1.04	7.36
Th/Sc	0.97	0.84	4.34	2.68	2.32	2.14	1.60	0.67	0.87	3.07	0.67	7.06
Cr/Th	2.17	5.19	1.21	4.71	2.53	2.68	2.07	7.87	5.69	4.33	0.25	18.51
Co/Th	0.71	105.96	0.36	1.15	0.44	1.04	0.98	0.41	0.43	44.30	0.19	275.07
(La/Yb) _N	6.38	15.11	4.96	9.82	8.53	3.54	2.56	4.57	3.82	8.09	2.56	17.23
(La/Sm) _N	3.28	6.91	3.40	3.56	4.35	2.10	2.02	1.21	1.05	3.81	1.05	6.91
(Gd/Yb) _N	1.36	1.19	1.05	1.83	1.38	1.29	1.02	0.46	0.50	1.30	0.46	2.16
Eu/Eu*	0.71	0.57	0.60	0.46	0.53	0.56	0.63	0.46	0.50	0.61	0.46	0.72

GQ = Gandikota Quartzite, Avg. = average, Min. = Minimum, Max. = Maximum.

Mg and Fe (Babechuk *et al.* 2014). Considering the redox-subordinate weathering of Fe, the MIA index is coordinated into two forms for oxidative (MIA-O) and lessened (MIA-R) weathering. Meunier *et al.* (2013) further established this method by incorporating SiO₂ into the index calculation and presented a weathering intensity scale (WIS). The WIS portrayed not only the Si-accumulation dominated kaolinization stage, but also the ultimate desilicification-dominated bauxitization/laterization stage for a general weathering procedure based on the co-variation between $R^{3+}/(R^{3+} + R^{2+} + M^+)$ ratio and $\Delta 4Si\%$ parameter (Yang *et al.* 2016). On the $R^{3+}/(R^{3+} + R^{2+} + M^+)$ vs. $\Delta 4Si\%$ diagram (Meunier *et al.* 2013; figure 9b), the studied sediments show the weathering trends from the felsic to mafic fields and intense chemical weathering. Furthermore, $M^{+} - 4Si - R^{2+}$ triangle diagram (Meunier *et al.* 2013; Yang *et al.* 2016; figure 9c) is used for the source rocks and weathering intensity of the source area. The majority of the studied sediments in this diagram plotted towards 4Si apex indicates intense weathering and source rocks from felsic to mafic.

Chemical Index of Weathering (CIW) of Harnois (1988) is also used to assess intensity of chemical weathering. It is considered as a better index than CIA because it does not include K₂O content and thus eliminate the possibility of K-metasomatism. It is calculated as:

$$CIW = [Al_2O_3 / (Al_2O_3 + CaO^* + Na_2O)] \times 100 \quad (2)$$

CIW values of the studied Pulivendla and Gandikota Quartzite range from 49.85 to 97.59 (avg. 91.21) and 80.44 to 97.60 (avg. 90.87), respectively. CIW indices are higher than CIA values for some analysed samples due to exclusion of K₂O from the index. On the basis of CIW, the studied sediments also show moderate to intense weathering.

One more fine evaluation method to determine the amount of chemical weathering is Plagioclase Index of Alteration (PIA; Fedo *et al.* 1995), which can be considered by the subsequent equation. In this, all oxides are expressed in molecular proportions

$$PIA = [(Al_2O_3 - K_2O) / (Al_2O_3 + CaO + Na_2O - K_2O)] \times 100 \quad (3)$$

PIA values of ~50 for fresh rocks and values similar to 100 designate considerable productions

of secondary aluminous clay minerals (Fedo *et al.* 1997). The PIA value of Pulivendla Quartzite is 37–96 (avg. 87) and Gandikota Quartzite is 70–96 (avg. 86). Like CIA, A–CN–K ternary diagram and CIW, the range of PIA values of all these quartzites also suggest moderate to intense chemical weathering.

The Index of Chemical Variability (ICV) can also be useful as an index for recycling and compositional maturity in sedimentary rocks (Cox *et al.* 1995; Armstrong-Altrin 2015)

$$ICV = (Fe_2O_3 + K_2O + Na_2O + CaO + MgO + MnO + TiO_2) / Al_2O_3 \quad (4)$$

ICV values of Pulivendla Quartzite range from 0.30 to 1.76 (avg. 0.57) reflect the high mature sediments recycled. The high ICV value (~1) reflects that the sediments were deposited as first cycle deposits in tectonically active continental margins. But Gandikota Quartzite are having the ICV range from 0.27 to 1.29 (avg. 0.69). The samples with ICV <1 are showing the signature of sediment recycling and highly mature. The samples with ICV >1 are indicating that these are first cycle of sediments and immature nature (table 2).

Similarly, the ICV vs. CIA plot (figure 9d, after Potter *et al.* 2005; LaMaskin *et al.* 2008; Absar and Sreenivas 2015) suggest that the source of the studied sediments is from predominantly granodiorite source rocks. However, some samples fall along the granite and basalt mixing line, indicating mixed igneous provenance. Virtually weak and non-enduring weathering condition in the source ranges are shown by the substantial inconstancy of CIA esteems and variable convergence of labile components, for example, Ca, Na, and Sr (Nesbitt *et al.* 1997). In this distinctive circumstance, we derive that these sediments were provided from a quickly uplifted source zone.

On the basis of the weathering indices like CIA, A–CN–K plot (figure 9a), CIW (Harnois 1988), PIA and ICV, ICV vs. CIA plot (figure 9d) of Pulivendla and Gandikota Quartzite, it has been suggested that these sediments suffered moderate to intense chemical weathering and are deposited in humid and warm climate. The low to moderate chemical weathering of these sediments is due to nonsteady state weathering conditions where active tectonism and uplift allow erosion of all soil horizons and rock surfaces (Nesbitt *et al.* 1997). Low to moderate chemical weathering in the quartzites

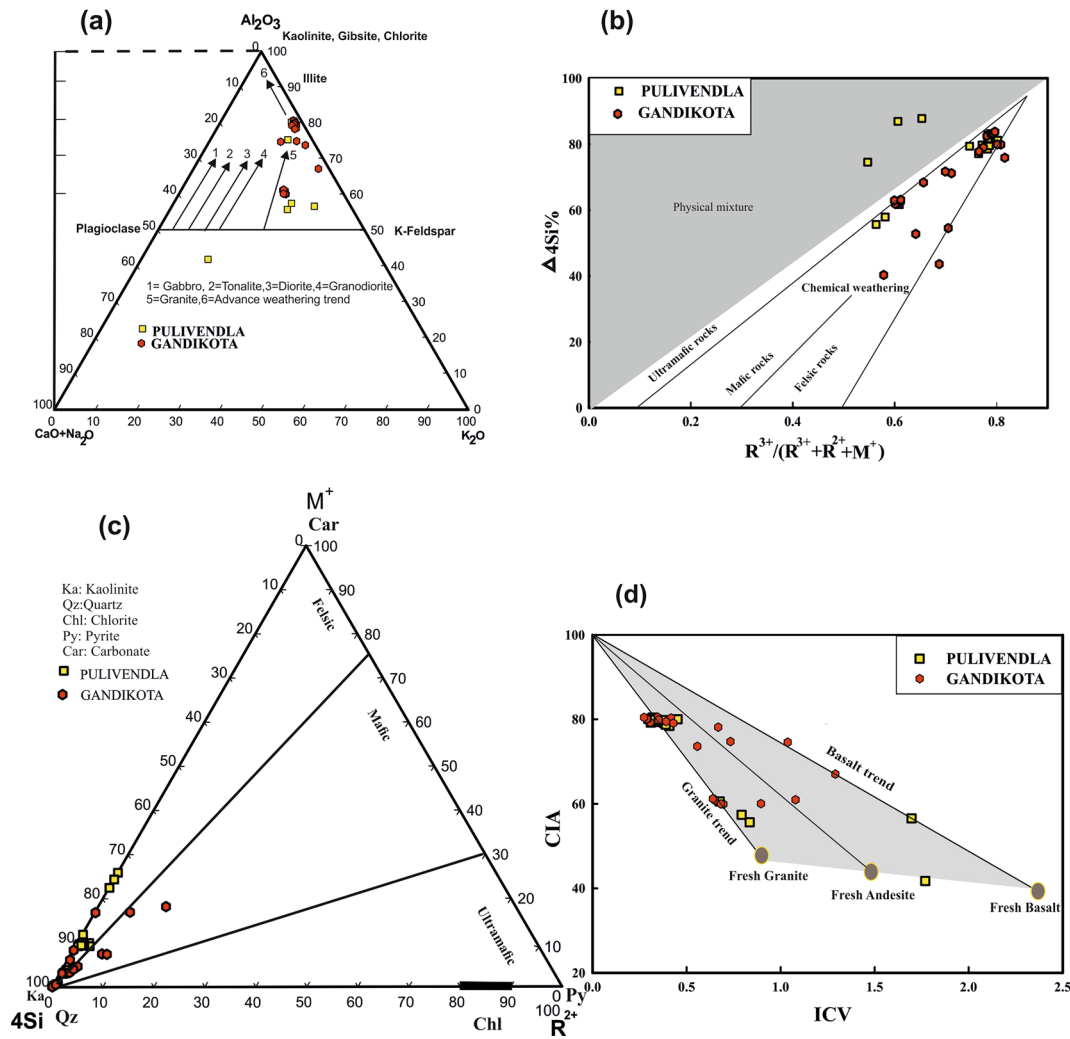


Figure 9. (a) A–CN–K ternary diagram of molecular proportions of Al_2O_3 –($CaO+Na_2O$)– K_2O for the Pulivendla and Gandikota Quartzite (after Nesbitt and Young 1984). (b) Chemiographic bases of the Weathering Alteration Scale (WIS). $M^+-4Si-R^{2+}$ ternary plot (fields after Meunier et al. 2013; Yang et al. 2016). (c) $R^{3+}/(R^{3+} + R^{2+} + M^+)$ vs. $\Delta 4Si\%$ for sediments of Chitravati Group. Calculation of monocationic molar proportions (ex. $Si = ((SiO_2) \times 1000)/60.09$), $4si = Si/4$ ($4Si\% = 39.8\%$ (average upper crust); $\Delta 4Si\% = (4Si\% \text{ sample } 39.8) \times 100/(100 - 39.8)$). Calculation of the R^{3+} , R^{2+} , and M^+ parameters $R^{3+} = Al^{3+} + Fe^{3+}$; $R^{2+} = Mg^{2+} + Fe^{2+} + Mn^{2+}$; $M^+ = Na^+ + K^+ + 2Ca^{2+}$ (fields after Meunier et al. 2013). (d) Two weathering indicators, Index of Chemical Variation (ICV) vs. Chemical Index of Alteration (CIA; fields after Potter et al. 2005).

of Pulivendla and Gandikota reflects high erosion rate giving less time to the debris to stay *in situ*.

Hydraulic sorting preserves the chemical composition of terrigenous sedimentary rocks and also dominantly controls the distribution of various trace elements (e.g., Th, U, Zr, Hf and Nb) (Etemad-Saeed et al. 2011). McLennan et al. (1993) used Th/Sc vs. Zr/Sc plot to discriminate the effects of source composition and sedimentary processes on the final composition of clastic sedimentary rocks. On the Th/Sc vs. Zr/Sc binary plot for quartzites two trends are observed, one showing a direct contribution from primary source rocks,

and the other revealing the influence of edimentary recycling (figure 10a). These sediments are enriched in heavy minerals particularly zircon due to sediment sorting and recycling. Similarly, these samples plot in the field of sub-parallel to trend one near the Proterozoic sandstones (Condie 1993) suggesting compositional heterogeneity and maximum influence of sorting and recycling by heavy minerals. Further, Th/U ratios of 3.5–4.0 in Th/U vs. Th plot indicates that the sediments are derived from upper crustal igneous rocks and if the Th/U ratios are below 3.5, they are supposed to have been derived from depleted mantle. Our quartzite

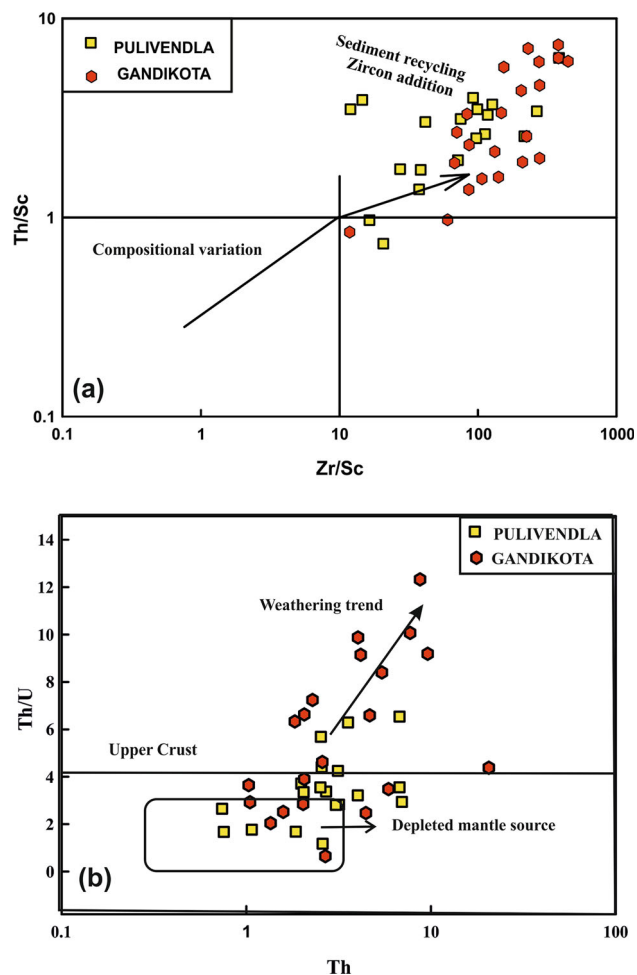


Figure 10. (a) Th/Sc vs. Zr/Sc diagram for Pulivendla and Gandikota Quartzite (McLennan *et al.* 1993). The accumulation of zircon due to sediment recycling and sorting is observed in trend 2 and compositional variation in trend 1. (b) Plot of Th/U vs. Th showing majority of samples low values of Th <10 and low Th/U ratio above four suggested upper crustal regions (after McLennan *et al.* 1993).

samples from Pulivendla and Gandikota reflect both the components. During the continuous sedimentary processes, lower Th/U ratios are usually the result of U enrichments found in active margin sediments, throughout the post-Archean terranes (McLennan *et al.* 1993). During the post-Archean, low Th/U ratios are likely to be a sign of origin of crustal precursors from depleted mantle sources. This is reflected in our samples (figure 10b).

6.2 Provenance

The chemical composition of sedimentary rocks is controlled by a complex suite of parameters operating through erosion, transport and deposition. The principal first-order parameters include

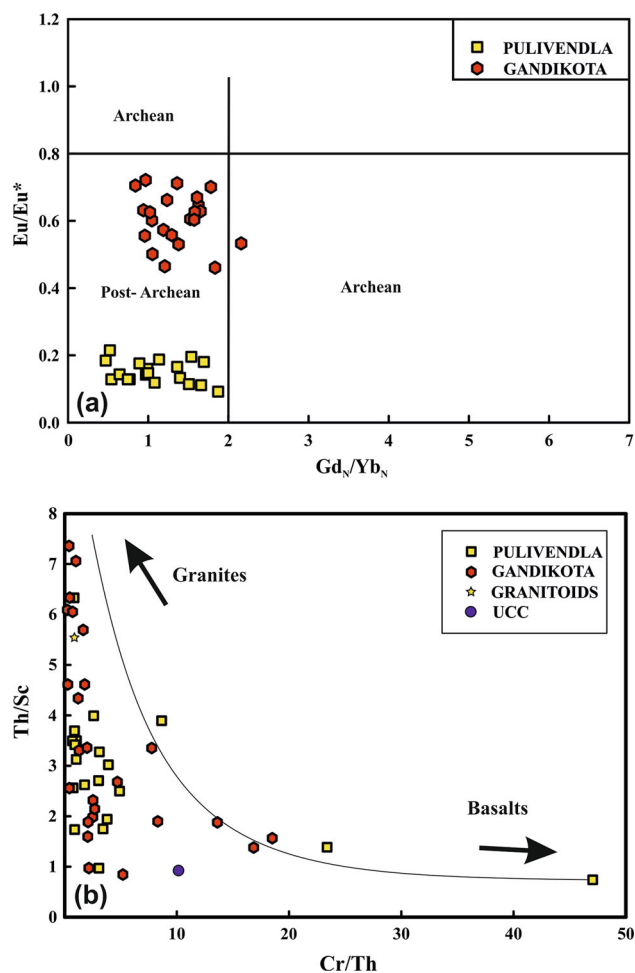


Figure 11. (a) Eu/Eu* vs. Gd_N/Yb_N plot showing all of our studied samples plotted in post-Archean field. (b) Th/Sc vs. Cr/Th plot (after Totten *et al.* 2000).

source rock composition, modification by chemical weathering, mechanical disaggregation and abrasion, authigenic inputs, hydraulic sorting, and diagenesis (Johnsson 1993; Walsh *et al.* 2016). For example, alkali and alkaline earth elements, such as K, Na, Ca and Sr may be transported as dissolved species and their abundances in sedimentary rocks may not reflect their abundances in source terrain (Sheldon *et al.* 2002). However, immobile elements such as Al₂O₃, Ti, Th, Ni, Cr, Co, Zr and REE are commonly transported in solid detritus and are reliable indicator of provenance (Holland 1978; Chaudhuri and Cullers 1979; Taylor and McLennan 1985; Totten and Blatt 1993). For the purpose of identification of the provenance, various major and trace element ratios like Al₂O₃/TiO₂, Th/Sc, La/Sc, La/Co, Co/Th, Cr/Th and Cr/Zr of the siliciclastic rocks are reliable provenance indicators (Bhatia and Crook 1986; Bauluz Lazaro *et al.* 1995; Cullers and Berendsen 1998). The Al₂O₃/TiO₂ for

Table 3. REE mixing calculations taking all averages 70% Tadpatri shale (A) + 30% Quartzite (B) as a sample and 40% Granitoid (G) + 40% Closepet granite (CG) + 20% Basalt (B) as a model.

Elements	Tadpatri			Closepet		Sample 70%A + 30%B	Model 40%G + 40%CG + 20%B
	Shales (A)	Quartzite (B)	Granitoid (G)	Granite (CG)	Basalt (B)		
La	167.85	20.46	116.14	301.39	8.57	123.63	168.73
Ce	117.55	17.73	98.41	237.13	9.15	87.60	101.85
Nd	65.65	10.87	51.26	122.30	9.76	49.22	54.50
Sm	37.71	6.28	28.15	60.23	10.02	28.28	29.82
Eu	20.17	3.27	22.74	32.82	10.37	15.10	20.93
Gd	22.04	4.60	16.62	30.26	10.85	16.81	18.01
Dy	12.95	4.40	11.17	16.87	10.77	10.39	12.45
Er	11.06	4.09	7.18	13.09	10.96	8.97	9.98
Yb	10.29	4.07	7.74	11.15	20.36	8.43	13.01
Lu	9.84	4.55	8.56	11.71	11.66	8.25	10.44
Eu/Eu*	0.70	0.62	1.05	0.77	0.99	0.68	0.96
(La/Sm) _N	4.45	3.31	4.13	5.00	0.86	4.11	3.20
(Gd/Yb) _N	2.14	1.00	2.15	2.71	0.53	1.80	1.72
(La/Yb) _N	16.31	4.37	15.00	27.04	0.42	12.73	12.91

the felsic rocks is generally ranging from 10 to 100 (sometimes higher), whereas for mafic rocks it is <20 (Hayashi *et al.* 1997). The Al₂O₃/TiO₂ ratio of the Pulivendla Quartzite (27.5–826.0, avg. 339.9) and Gandikota Quartzite (6.33–831.0, avg. 215), which suggest that sediments are derived dominantly from felsic source with minor proportion from mafic or ultramafic source rocks. Cullers and Podkovyrov (2000) suggested various trace element ratios for coarse and fine grained rocks for the provenance purpose. Coarse grained sediments have Th/Sc range for felsic rocks 0.84 to 20.5 and for basic rocks 0.05 to 0.22 and La/Sc ratio for felsic rocks 2.5 to 16.3 and for basic rocks 0.43 to 0.86. Coarse grained sediments derived from felsic sources have Th/Cr values ranging from 0.13 to 2.7 and basic rock 0.018 to 0.046 (Cullers and Podkovyrov 2000 and references therein). The trace element ratios of Pulivendla Quartzite are Th/Sc (0.74–6.33, avg. 2.84), La/Sc (0.79–12.83, avg. 4.44), Th/Cr (0.02–1.44, avg. 0.63) and V/Ni (0.47–5.65, avg. 1.98) and for Gandikota Quartzite are Th/Sc (0.84–7.36, avg. 3.45), La/Sc (1.04–6.27, avg. 3.32), Th/Cr (0.05–4.05, avg. 1.0) and V/Ni (0.13–5.74, avg. 1.35). On the basis of these trace element ratios of Pulivendla and Gandikota Quartzite, we are inferring here that sediments of Pulivendla and Gandikota Quartzite-are derived dominantly from felsic source with minor contribution from mafic source.

Furthermore the quartzites of Pulivendla and Gandikota have negative Eu/Eu* (Pulivendla:

0.09–0.21, avg. 0.15; Gandikota: 0.46–0.72, avg. 0.61) with high La_N/Yb_N ratio (0.71–16.63, avg. 5.36, for Pulivendla; 2.56–17.23, avg. 8.09, for Gandikota). Felsic rocks generally have negative Eu anomaly and high La_N/Yb_N ratios, whereas mafic rocks have low La_N/Yb_N ratios (McLennan *et al.* 1990). In the chondrite normalised REE patterns of both quartzites showing LREE enriched with flat HREE and few samples with concave upward HREE patterns (figure 8a and b). The REE patterns and their ratios of our samples also suggest a heterogeneous source comprising felsic dominant component with minor proportion of mafic component.

The Gd_N/Yb_N ratio also document the nature of source rocks and the composition of the continental crust (Taylor and McLennan 1985; Nagarajan *et al.* 2007). On Eu/Eu* *vs.* Gd_N/Yb_N diagram (figure 11a, fields after McLennan *et al.* 1993), all our samples plot in post-Archean field, near to PAAS values. The studied sediments are also plotted in Cr/Th *vs.* Th/Sc plot (Totten *et al.* 2000; figure 11b) and La/Th *vs.* Hf (Floyd and Leveridge 1987) in which samples showing mixed provenance (figure 12a) source.

The provenance modelling using chondrite normalised REEs have been established to be a valuable tool for determining the contribution of possible end-members to the sedimentary basin (e.g., Hofmann 2005; Roddaz *et al.* 2007). In this provenance modelling it is necessary that mass balance should be taken into consideration. It is

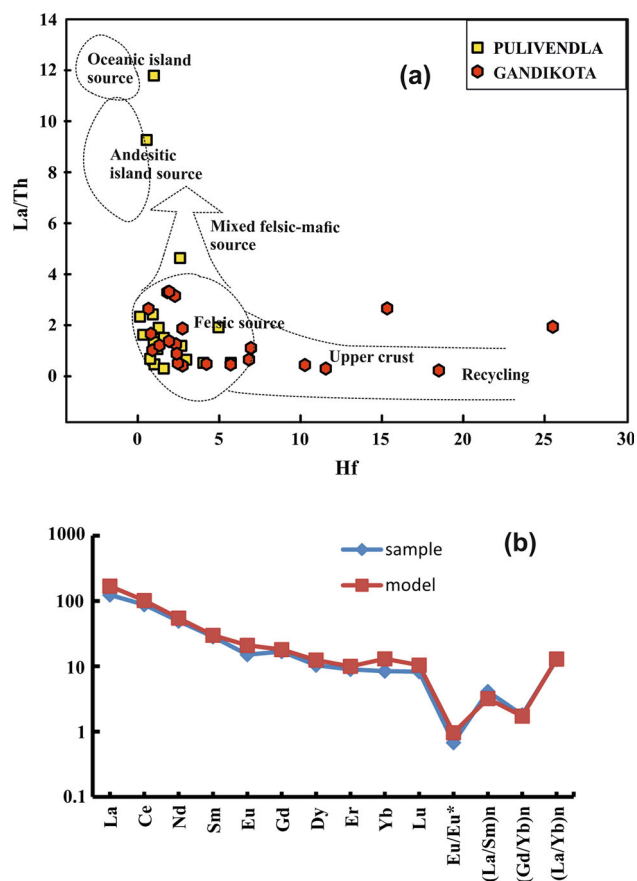


Figure 12. (a) La/Th vs. Hf diagram of source rock discrimination for the discussion of the clastic sediments and their compositions reflects the mixed felsic-mafic source. (b) Chondrite-normalized REE patterns of average Chitravati Group siliciclastics compared with models after mixing the end-members in the proportion of 40% G: 40% CG: 20% B. Granitoids (G; Dey *et al.* 2014), Closepet Granite (CG; Moyen *et al.* 2001) and Basalt (B; Manikyamba *et al.* 2004).

known that pelitic rocks (shale) and sandstone include 70 and 30%, respectively of the total mass of sediments (Mackenzie and Garrels 1971; Taylor and McLennan 1985), consequently a mixture of 70% shale and 30% sandstone is taken as model composition. Shale unit from Tadpatri Formation (Ramavathi Mathur *et al.* 1995), which is the Chitravati Group is used for mixing model. Components of the Dharwar craton like Granitoids (G; Dey *et al.* 2014), Closepet Granite (CG; Moyen *et al.* 2001) and Basalt (B; Manikyamba *et al.* 2004) have been taken as end members for the function of modelling of Chitravati Group. The mixing calculations from these end members suggest a possible model for Chitravati siliciclastics in the proportions of 40% G: 40% CG: 20% B (table 3). The chondrite normalised REE patterns and their ratios

are near matching to those of average sediments of Chitravati siliciclastics (figure 12b) and are in agreement with presently exposed proportion of the end-members of the respective sources. Even though this mixing model does not yield an exceptional solution, it positively specifies contribution of source terrain rare earth element abundance for the genesis of sedimentary rocks of the Chitravati Group.

Geochronological studies on Chitravati Group are showing the 1923 ± 22 Ma (Collins *et al.* 2015) as a consistent maximum depositional age for the Pulivendla Formation. This information is in agreement with the present geochemical studies, which infer Dharwar cratonic rocks as a Provenance for the Pulivendla Formation. The Gandikota Formation yields the maximum depositional age of 1181 ± 29 Ma (Collins *et al.* 2015) and the provenance was inferred to be the Krishna orogeny (Collins *et al.* 2015). The Paleocurrent analysis (Nagaraja Rao 1974; Lakshminarayana and Bhat-tacharjee 2000) is supporting the Dharwar cratonic rocks as a Provenance. The bi-modal Paleocurrent directions noticed by Lakshminarayana and Bhat-tacharjee (2000) indicate the provenance of the Gandikota Formation should be two directional of which one direction supports geochronological evidence (Collins *et al.* 2015; 1181 ± 29 Ma), i.e., sediments were also derived from Krishna orogeny and the other paleocurrent direction was supporting the Dharwar craton source. Our petrological, geochemical and provenance modelling studies show that the Gandikota Quartzite were derived from a mixed component source involving both Dharwar and Krishna Orogeny (by earlier isotopic studies by Collins *et al.* 2015).

6.3 Tectonic setting

Sediments derived from different tectonic settings vary in different geochemical characteristics. Major and trace-element and their different bivariate and multivariate diagrams with discrimination functions are predominantly valid for tectonic setting of the sedimentary basins (Bhatia 1983; Roser and Korsch 1986). Major element discrimination function diagram of Bhatia (1983) for the studied samples of Pulivendla and Gandikota Quartzite are showing passive to active continental margin setting (figure 13a).

Recently, Verma and Armstrong-Altrin (2013) proposed two discriminant function diagrams based on major elements for the tectonic discrimination

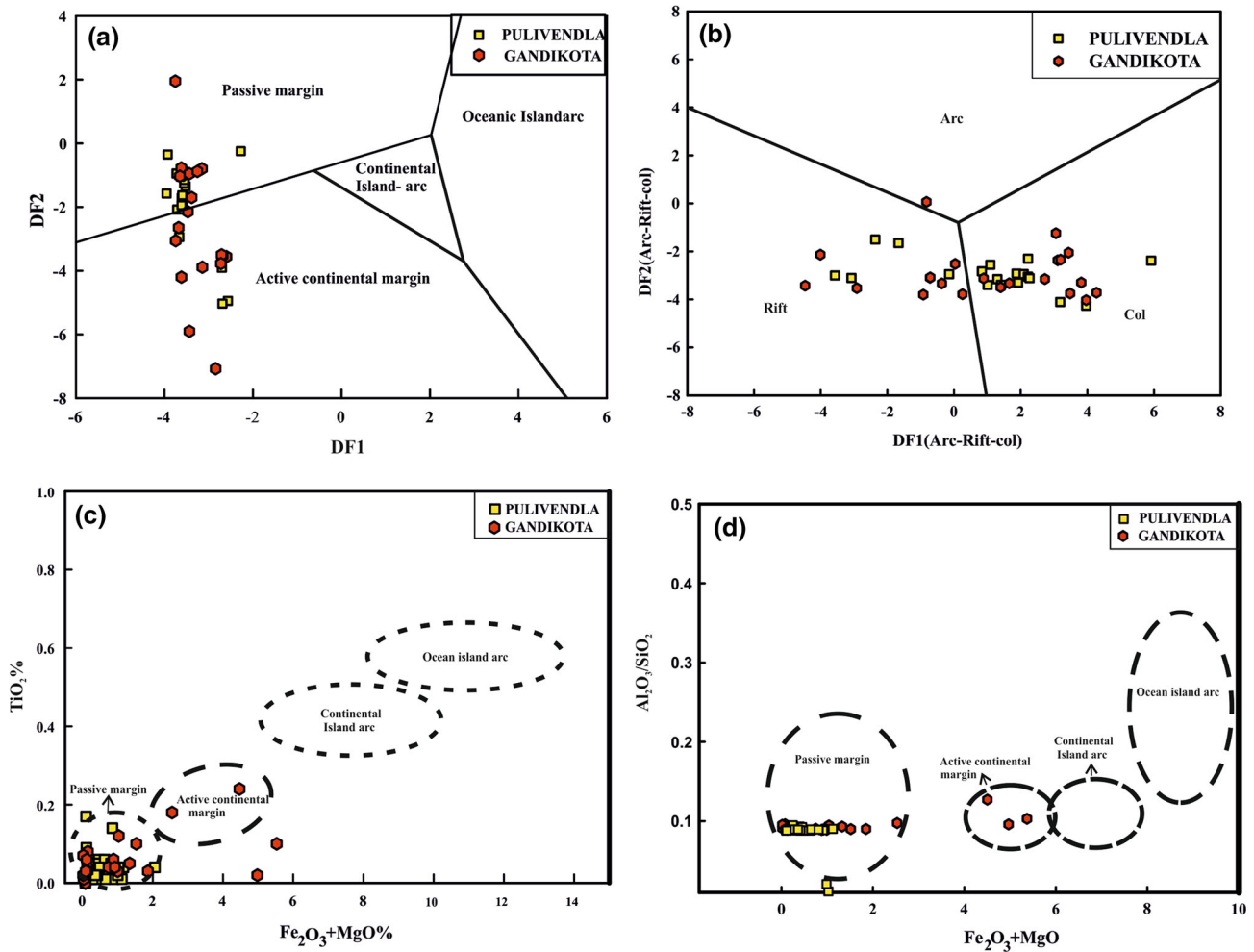


Figure 13. (a) Discrimination function plot of the Pulivendla, Gandikota Quartzite (fields after [Bhatia 1983](#)). Discriminant function 1 (DF1) = $-0.0447\text{SiO}_2 - 0.972\text{TiO}_2 + 0.008\text{Al}_2\text{O}_3 - 0.267\text{Fe}_2\text{O}_3 + 0.208\text{FeO} - 3.082\text{MnO} + 0.140\text{MgO} + 0.195\text{CaO} + 0.719\text{Na}_2\text{O} - 0.032\text{K}_2\text{O} + 7.510\text{P}_2\text{O}_5 + 0.303$. Discriminant function 2 (DF2) = $-0.421\text{SiO}_2 + 1.988\text{TiO}_2 - 0.526\text{Al}_2\text{O}_3 - 0.551\text{Fe}_2\text{O}_3 - 1.610\text{FeO} + 2.720\text{MnO} + 0.881\text{MgO} - 0.907\text{CaO} - 0.177\text{Na}_2\text{O} - 1.840\text{K}_2\text{O} + 7.244\text{P}_2\text{O}_5 + 43.57$. (b) Discriminant function multidimensional diagram for high-silica clastic sediments ([Verma and Armstrong-Altrin 2013](#)). The discriminant function equations are: $\text{DF1(Arc-Rift-Col)} = (-0.263 \times \ln(\text{TiO}_2/\text{SiO}_2)\text{adj}) + (0.604 \times \ln(\text{Al}_2\text{O}_3/\text{SiO}_2)\text{adj}) + (-1.725 \times \ln(\text{Fe}_2\text{O}_3/\text{SiO}_2)\text{adj}) + (0.660 \times \ln(\text{MnO}/\text{SiO}_2)\text{adj}) + (2.191 \times \ln(\text{MgO}/\text{SiO}_2)\text{adj}) + (0.144 \times \ln(\text{CaO}/\text{SiO}_2)\text{adj}) + (-1.304 \times \ln(\text{Na}_2\text{O}/\text{SiO}_2)\text{adj}) + (0.054 \times \ln(\text{K}_2\text{O}/\text{SiO}_2)\text{adj}) + (-0.330 \times \ln(\text{P}_2\text{O}_5/\text{SiO}_2)\text{adj}) + 1.588$. $\text{DF2(Arc-Rift-Col)} = (-1.196 \times \ln(\text{TiO}_2/\text{SiO}_2)\text{adj}) + (1.604 \times \ln(\text{Al}_2\text{O}_3/\text{SiO}_2)\text{adj}) + (0.303 \times \ln(\text{Fe}_2\text{O}_3/\text{SiO}_2)\text{adj}) + (0.436 \times \ln(\text{MnO}/\text{SiO}_2)\text{adj}) + (0.838 \times \ln(\text{MgO}/\text{SiO}_2)\text{adj}) + (-0.407 \times \ln(\text{CaO}/\text{SiO}_2)\text{adj}) + (1.021 \times \ln(\text{Na}_2\text{O}/\text{SiO}_2)\text{adj}) + (-1.706 \times \ln(\text{K}_2\text{O}/\text{SiO}_2)\text{adj}) + (-0.126 \times \ln(\text{P}_2\text{O}_5/\text{SiO}_2)\text{adj}) - 1.068$. (c) Plots of major oxide data in the different tectonic setting discrimination diagrams. Plot of $(\text{Fe}_2\text{O}_3 + \text{MgO})$ vs. TiO_2 content (fields after [Bhatia 1983](#)). (d) Plot of $(\text{Fe}_2\text{O}_3 + \text{MgO})$ vs. $(\text{Al}_2\text{O}_3/\text{SiO}_2)$ (after [Bhatia 1983](#)). Note that the majority of the sample plots are close to the passive margin field.

of low and high silica rich sediments. In these diagrams there are three major different tectonic setting fields, viz., continental arc (island arc), continental rift and collision. Present studied samples are all high-silica sediments, which are plotted in the rift and collisional fields of discriminant function multidimensional diagram of Verma and Armstrong-Altrin (2013; figure 13b).

Similarly, the plot of $\text{Fe}_2\text{O}_3 + \text{MgO}$ vs. TiO_2 (figure 13c; [Bhatia 1983](#); [Basu et al. 2016](#));

$\text{Fe}_2\text{O}_3 + \text{MgO}$ vs. $\text{Al}_2\text{O}_3/\text{SiO}_2$ (figure 13d; [Bhatia 1983](#)), tectonic setting diagram reflecting the both of the studied sediments are plotted in passive margin setting except four samples of Gandikota Quartzite showing active continental margin settings. Corroborating with major element data, the trace element ternary diagram Th–Sc–Zr/10 of the studied samples of Pulivendla and Gandikota, is showing passive to active tectonic setting (figure 14).

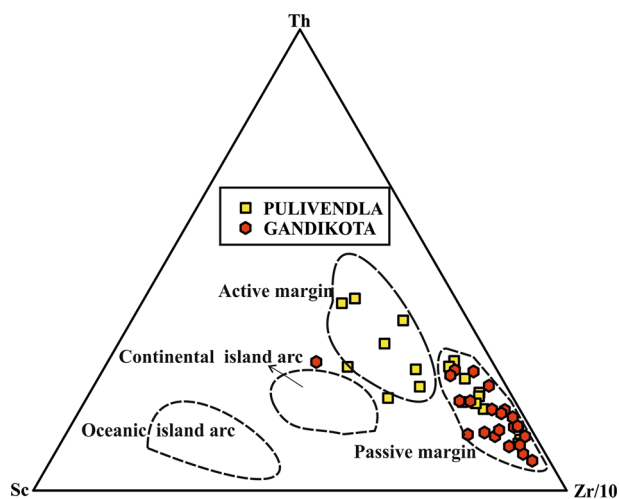


Figure 14. Th–Sc–Zr/10 ternary diagram for Pulivendla and Gandikota Quartzite of Chitravati Group (after Bhatia and Crook 1986).

7. Conclusions

1. On the basis of petrography and ICV the quartzites of Chitravati Group are mostly well sorted, texturally and compositionally mature. The CIA, PIA, CIW, WIS and ACNK ternary diagram suggests that these quartzites have undergone moderate to intense chemical weathering in their source area.
2. Discrimination function diagrams and ternary diagram show passive to active continental margin setting in conjunction with contemporaneous volcanism and sedimentation.
3. Based on geochemical provenance modelling studies of Chitravati Group quartzites (Cuddapah Supergroup), it is suggested that granitoid terrains to the north, west and south of the Cuddapah basin are the source of these quartzites as suggested by earlier workers.

Acknowledgements

The authors sincerely thank Dr. V M Tiwari, Director, CSIR-NGRI Hyderabad for permitting us to publish this work. Drs. C Manikyamba, M Ram Mohan, and Tavheed Khan are thanked for helpful discussions. This work was carried out with Institute funding under MLP-6201-28 (CM). VSS acknowledges Dr. B K Nagaraja Rao, Former Director GSI for his guidance during field studies. This work forms part of VSS Ph.D. thesis.

References

- Absar N and Sreenivas B 2015 Petrology and geochemistry of greywackes of the ~1.6 Ga Middle Aravalli Supergroup, northwest India: Evidence for active margin processes; *Int. Geol. Rev.* **57**(2) 134–158.
- Absar N, Nizamudheen B M, Augustine S, Managave S and Balakrishnan S 2016 C, O, Sr and Nd isotope systematics of carbonates of Papaghni sub-basin, Andhra Pradesh, India: Implications for genesis of carbonate-hosted stratiform uranium mineralisation and geodynamic evolution of the Cuddapah basin; *Lithos* **263** 88–100.
- Absar N, Raza M, Roy M, Naqvi S M and Roy A K 2009 Composition and weathering conditions of Paleoproterozoic upper crust of Bundelkhand craton, central India: Records from geochemistry of clastic sediments of 1.9 Ga Gwalior Group; *Precamb. Res.* **168**(3) 313–329.
- Anand M, Gibson S A, Subbarao K V, Kelley S P and Dickin A P 2003 Early Proterozoic melt generation processes beneath the intra-cratonic Cuddapah Basin, southern India; *J. Petrol.* **44**(12) 2139–2171.
- Armstrong-Altrin J S 2015 Evaluation of two multi-dimensional discrimination diagrams from beach and deep-sea sediments from the Gulf of Mexico and their application to Precambrian clastic sedimentary rocks; *Int. Geol. Rev.* **57**(11–12) 1446–1461.
- Babechuk M G, Widdowson M and Kamber B S 2014 Quantifying chemical weathering intensity and trace element release from two contrasting basalt profiles, Deccan Traps, India; *Chem. Geol.* **363** 56–75.
- Basu A, Bickford M E and Deasy R 2016 Inferring tectonic provenance of siliciclastic rocks from their chemical compositions: A dissent; *Sedim. Geol.* **336** 26–35.
- Basu H, Sastry R S, Achar K K, Umamaheswar K and Parihar P S 2014 Paleoproterozoic fluvio-aeolian deposits from the lower Gulcheru Formation, Cuddapah Basin, India; *Precamb. Res.* **246** 321–333.
- Bauluz Lazaro B, Mayayo Burillo M J, Fernandez-Nieto C and Gonzalez Lopez J M 1995 Mineralogy and geochemistry of Devonian detrital rocks from the Iberian Range (Spain); *Clay Miner.* **30**(4) 381–394.
- Bhatia M R and Crook K A W 1986 Trace element characteristics of greywackes and tectonic settling discriminations of sedimentary basins; *Contrib. Mineral. Petrol.* **92** 181–193.
- Bhatia M R 1983 Plate tectonics and geochemical composition of sandstones; *J. Geol.* **91**(6) 611–627.
- Chakrabarti G, Shome D, Bauluz B and Sinha S 2009 Provenance and weathering history of Mesoproterozoic clastic sedimentary rocks from the basal Gulcheru Formation, Cuddapah Basin; *J. Geol. Soc. India* **74**(1) 119–130.
- Chaudhuri S and Cullers R L 1979 The distribution of rare-earth elements in deeply buried Gulf Coast sediments; *Chem. Geol.* **4**(3–4) 327–338.
- Collins A S, Patranabis-Deb S, Alexander E, Bertram C N, Falster G M, Gore R J, Mackintosh J, Dhang P C, Saha D, Payne J L, Jourdan F, Backé G, Halverson G P and Wade B P 2015 Detrital mineral age, radiogenic isotopic stratigraphy and tectonic significance of the Cuddapah Basin, India; *Gondwana Res.* **28**(4) 1294–1309.

- Condie K C 1993 Chemical composition and evolution of the upper continental crust: Contrasting results from surface samples and shales; *Chem. Geol.* **104**(1–4) 1–37.
- Condie K C, Des Marais D J and Abbott D 2001 Precambrian superplumes and supercontinents: A record in black shales, carbon isotopes, and paleoclimate?; *Precamb. Res.* **106**(3) 239–260.
- Cox R, Lowe D R and Cullers R L 1995 The influence of sediment recycling and basement composition on evolution of mudrock chemistry in the southwestern United States; *Geochim. Cosmochim. Acta* **9**(14) 2919–2940.
- Cullers R L and Podkovyrov V N 2000 Geochemistry of the Mesoproterozoic Lakhanda shales in southeastern Yakutia, Russia: implications for mineralogical and provenance control, and recycling; *Precamb. Res.* **104**(1) 77–93.
- Cullers R L and Podkovyrov V N 2002 The source and origin of terrigenous sedimentary rocks in the Mesoproterozoic Ui group, southeastern Russia; *Precamb. Res.* **117**(3) 157–183.
- Cullers R L and Berendsen P 1998 The provenance and chemical variation of sandstones associated with the Mid-Continent Rift system, USA; *Eur. J. Mineral.* **10** 987–1002.
- Dasch E J 1969 Strontium isotopes in weathering profiles, deep-sea sediments, and sedimentary rocks; *Geochim. Cosmochim. Acta* **33**(12) 1521–1552.
- Dasgupta P K, Biswas A and Mukherjee R 2005 Cyclicity in paleoproterozoic to neoproterozoic cuddapah supergroup and its significance in basinal evolution; *Dev. Sedimentol.* **57** 313–354.
- Dey S, Nandy J, Choudhary A K, Liu Y and Zong K 2014 Origin and evolution of granitoids associated with the Kadiri greenstone belt, eastern Dharwar craton: A history of orogenic to an orogenic magmatism; *Precamb. Res.* **246** 64–90.
- Dickinson W R 1985 *Interpreting provenance relations from detrital modes of sandstones*; Provenance of arenites, Springer, Dordrecht, pp. 333–361.
- Erickson K A, Taylor S R and Korsch R J 1992 Geochemistry of 1.8–1.67 Ga mudstones and siltstones from the Mount Isa Inlier, Queensland Australia: Provenance and tectonic implications; *Geochim. Cosmochim. Acta* **56**(3) 899–909.
- Etemad-Saeed N A, Hosseini-Barzi M A and Armstrong-Altrin J S 2011 Petrography and geochemistry of clastic sedimentary rocks as evidences for provenance of the Lower Cambrian Lalun Formation, Posht-e-badam block, central Iran; *J. Afr. Earth. Sci.* **61**(2) 142–159.
- Fedo C M, Nesbitt H W and Young G M 1995 Unravelling the effects of potassium metasomatism in sedimentary rocks and paleosols, with implications for paleoweathering conditions and provenance; *Geology* **23**(10) 921–924.
- Fedo C M, Young G M and Nesbitt H W 1997 Paleoclimatic control on the composition of the Paleoproterozoic Serpent Formation, Huronian Supergroup, Canada: A greenhouse to icehouse transition; *Precamb. Res.* **86**(3–4) 201–223.
- Floyd P A and Leveridge B E 1987 Tectonic environment of the Devonian Gramscatho basin, south Cornwall: Framework mode and geochemical evidence from turbiditic sandstones; *J. Geol. Soc.* **144**(4) 531–542.
- Folk R L 1974 *Petrology of sedimentary rocks*; Hemphill Publishing Company, Austin.
- French J E, Heaman L M, Chacko T and Srivastava R K 2008 1891–1883 Ma southern Bastar–Cuddapah mafic igneous events, India: A newly recognized large igneous province; *Precamb. Res.* **160**(3) 308–322.
- Goodwin A M 1996 *Principles of Precambrian geology*; Academic Press, London, ISBN: 978-0-12-289770-2.
- Harnois L 1988 The CIW index: A new chemical index of weathering; *Sedim. Geol.* **55** 319–322.
- Hayashi K, Fujisawa H, Holland H D and Ohmoto H 1997 Geochemistry of ~1.9 Ga sedimentary rocks from northeastern Labrador, Canada; *Geochim. Cosmochim. Acta* **61** 4115–4137.
- Hofmann A 2005 The geochemistry of sedimentary rocks from the Fig Tree Group, Barberton greenstone belt: Implications for tectonic, hydrothermal and surface processes during mid-Archaean times; *Precamb. Res.* **143**(1) 23–49.
- Holland H D 1978 *Chemistry of the Atmosphere and Oceans*; Wiley, New York, 351p.
- Jayananda M T, Kano J, Peucat J and Capdevila R 2008 *Precamb. Res.*; *Precamb. Res.* **162** 160–179.
- Johnsson M J 1993 The system controlling the composition of clastic sediments; *Geol. Soc. Spec. Publ.* **284** 1–20.
- Joy S, Jelsma H, Tappe S and Armstrong R 2015 SHRIMP U–Pb zircon provenance of the Sullavai Group of Pranhita–Godavari Basin and Bairenkonda Quartzite of Cuddapah Basin, with implications for the southern Indian Proterozoic tectonic architecture; *J. Asian Earth Sci.* **11** 827–839.
- Khan T and Khan M S 2015 Clastic rock geochemistry of Punagarh basin, trans-Aravalli region, NW Indian shield: Implications for paleoweathering, provenance, and tectonic setting; *Arab. J. Geosci.* **8**(6) 3621–3644.
- Khan T and Khan M S 2016 Geochemistry of the sandstones of Punagarh basin: Implications for two source terranes and Arabian–Nubian connection of Aravalli craton?; *J. Geol. Soc. India* **88**(3) 366–386.
- King W 1872 On the Kadapah and Karnul formations in the Madras Presidency; *Gov. India* **8** 1–346 (part-1).
- Krishna A K, Murthy N N and Govil P K 2007 Multi-element analysis of soils by wavelength-dispersive X-ray fluorescence spectrometry; *Atom. Spectrosc.* **28**(6) 202.
- Kumar A, Gopalan K, Rao K R P and Nayak S S 2001 Rb–Sr ages of kimberlites and lamproites from Eastern Dharwar craton, south India; *J. Geol. Soc. India* **58** 135–142.
- Lakshminarayana G and Bhattacharjee S 2000 Shallow marine siliciclastic sedimentation in the middle Proterozoic Gandikota Formation, Cuddapah Basin, Andhra Pradesh; *J. Geol. Soc. India* **55**(1) 65–76.
- Lakshminarayana G, Bhattacharjee S and Ramanaidu K V 2001 Sedimentation and stratigraphic framework in the Cuddapah basin; *Geol. Surv. India Spec. Publ.* **55** 31–58.
- LaMaskin T A, Dorsey R J and Vervoort J D 2008 Tectonic controls on mudrock geochemistry, Mesozoic rocks of eastern Oregon and western Idaho, USA: Implications for cordilleran tectonics; *J. Sediment. Res.* **78**(12) 765–783.
- Mackenzie F T and Garrels R M 1971 *Evolution of sedimentary rocks*; Norton, New York.
- Manikyamba C, Kerrich R, Naqvi S M and Mohan M R 2004 Geochemical systematics of tholeiitic basalts from the 2.7 Ga Ramagiri–Hungund composite greenstone belt, Dharwar craton; *Precamb. Res.* **134**(1) 21–39.

- Martin A 2015 Tectonics of the Cuddapah Basin and a model of its evolution: A review; *Geol. Soc. Lond. Mem.* **43(1)** 231–254.
- McDonough W F and Sun S S 1995 The composition of the Earth; *Chem. Geol.* **120(3–4)** 223–253.
- McLennan S M and Taylor S R 1991 Sedimentary rocks and crustal evolution: Tectonic setting and secular trends; *J. Geol.* **99(1)** 1–21.
- McLennan S M, Hemming S, McDaniel D K and Hanson G N 1993 Geochemical approaches to sedimentation, provenance, and tectonics; *Geol. Soc. London Spec. Publ.* **284** 21–40.
- McLennan S M, Taylor S R, McCulloch M T and Maynard J B 1990 Geochemical and Nd–Sr isotopic composition of deep-sea turbidites: Crustal evolution and plate tectonic associations; *Geochim. Cosmochim. Acta* **54(7)** 2015–2050.
- Meijerink A M J, Rao D P and Rupke J 1984 Stratigraphic and structural development of the Precambrian Cuddapah Basin, SE India; *Precamb. Res.* **26(1)** 57–104.
- Meunier A, Caner L, Hubert F, El Albani A and Prêt D 2013 The weathering intensity scale (WIS): An alternative approach of the chemical index of alteration (CIA); *Am. J. Sci.* **313(2)** 113–143.
- Middelburg J J, van der Weijden C H and Woittiez J R 1988 Chemical processes affecting the mobility of major, minor and trace elements during weathering of granitic rocks; *Chem. Geol.* **68(3)** 253–273.
- Moyen J F, Martin H and Jayananda M 2001 Multi-element geochemical modelling of crust–mantle interactions during Late-Archaean crustal growth: The Closepet granite (south India); *Precamb. Res.* **112(1)** 87–105.
- Nagaraja Rao B K 1974 Geological mapping of the Gandikota hill range in Cuddapah and Kurnool district, A.P.; *Geol. Surv. India*, Unpublished Progress Report.
- Nagaraja Rao B K, Rajurkar S T, Ramalingaswamy G and Ravindra Babu 1987 Stratigraphy and structure and evolution of the Cuddapah Basin; *Geol. Soc. India Memoir* **6** 33–86.
- Nagarajan R, Armstrong-Altrin J S, Nagendra R, Madhavaraju J and Moutte J 2007 Petrography and geochemistry of terrigenous sedimentary rocks in the Neoproterozoic Rabanpalli Formation, Bhima Basin, southern India: Implications for paleoweathering conditions, provenance and source rock composition; *J. Geol. Soc. India* **70(2)** 297–312.
- Nesbitt H W and Young G M 1982 Early Proterozoic climates and plate motions inferred from major element chemistry of lutites; *Nature* **299** 715–717.
- Nesbitt H W and Young G M 1984 Prediction of some weathering trends of plutonic and volcanic rocks based on thermodynamic and kinetic considerations; *Geochim. Cosmochim. Acta* **48(7)** 1523–1534.
- Nesbitt H W and Young G M 1996 Petrogenesis of sediments in the absence of chemical weathering: Effects of abrasion and sorting on bulk composition and mineralogy; *Sedimentology* **43(2)** 341–358.
- Nesbitt H W, Fedo C M and Young G M 1997 Quartz and feldspar stability, steady and non-steady-state weathering, and petrogenesis of siliciclastic sands and muds; *J. Geol.* **105(2)** 173–192.
- Patranabis-Deb S, Saha D and Tripathy V 2012 Basin stratigraphy, sea-level fluctuations and their global tectonic connections: Evidence from the Proterozoic Cuddapah Basin; *Geol. J.* **47(2–3)** 263–283.
- Pettijohn F J, Potter P E and Siever R 1987 *Sand and Sandstones*; Springer, New York, 553p.
- Potter P E, Maynard J B and Depetris P J 2005 *Mud and mudstones: Introduction and overview*; Springer, Berlin.
- Ramavathi Mathur, Uday Raj B, Govil P K, Manikyamba C, Balaram V and Naqvi S M 1995 Geochemistry and depositional environments in Cuddapah basin, India; *Annu. Conven. Tirupati Geol. Soc. India*, pp. 105–108.
- Rao N V C, Miller J A, Pyle D M and Madhavan V 1996 New Proterozoic K–Ar ages for some kimberlites and lamproites from the Cuddapah Basin and Dharwar Craton, South India: Evidence for non-contemporaneous emplacement; *Precamb. Res.* **79(3–4)** 363–369.
- Rao N V C, Gibson S A, Pyle D M, Miller J A and Madhavan V 1999 Precise $^{40}\text{Ar}/^{39}\text{Ar}$ age determinations of the Kotakonda Kimberlite and Chelima Lamproite, India: Implication to the timing of Mafic Dyke Swarm emplacement in the eastern Dharwar Craton; *J. Geol. Soc. India* **53(4)** 425–432.
- Rao N V C, Wu F-Y and Srinivas M 2012 Mesoproterozoic emplacement and enriched mantle derivation of the Racherla alkali syenite, Palaeo-Mesoproterozoic Cuddapah Basin, southern India: Insights from in situ Sr–Nd isotopic analysis on apatite; In: Palaeoproterozoic of India (eds) Mazumder R and Saha D, *Geol. Soc. Spec. Publ.* **365** 185–195.
- Reddy V P, Reddy N S and Prasad C V R K 1990 Quartzites of the Cuddapah Group and their environment of deposition; *J. Geol. Soc. India* **35(4)** 408–420.
- Roddaz M, Debat P and Nikiema S 2007 Geochemistry of Upper Birimian sediments (major and trace elements and Nd–Sr isotopes) and implications for weathering and tectonic setting of the Late Paleoproterozoic crust; *Precamb. Res.* **159(3)** 197–211.
- Roser B P and Korsch R J 1988 Provenance signatures of sandstone–mudstone suites determined using discriminant function analysis of major-element data; *Chem. Geol.* **67(1–2)** 119–139.
- Roser B P and Korsch R J 1986 Determination of tectonic setting of sandstone–mudstone suites using content and ratio; *J. Geol.* **94(5)** 635–650.
- Sageman B B and Lyons T W 2005 Geochemistry of fine-grained sediments and sedimentary rocks, ‘Sediments, Diagenesis, and Sedimentary Rocks’ In: *Treatise on Geochemistry*, 2nd edn, Elsevier, New York **7**, pp. 115–158.
- Saha D and Chakraborty S 2003 Deformation pattern in the Kurnool and Nallamalai Groups in the northeastern part (Palnad Area) of the Cuddapah Basin, south India and its implication on Rodinia/Gondwana tectonics; *Gondwana Res.* **6(4)** 573–583.
- Saha D and Patranabis-Deb S 2014 Proterozoic evolution of Eastern Dharwar and Bastar cratons, India – an overview of the intracratonic basins, craton margins and mobile belts; *J. Asian Earth Sci.* **91** 230–251.
- Saha D and Tripathy V 2012 Paleoproterozoic sedimentation in the Cuddapah Basin, south India and regional tectonics: A review; *Geol. Soc. Spec. Publ.* **365(1)** 161–184.

- Saha D, Chakraborti S and Tripathy V 2010 Intracontinental thrusts and inclined transpression along eastern margin of the East Dharwar Craton, India; *J. Geol. Soc. India* **75** 323–337
- Sai V V S 2014 Pyroclastic volcanism in Papagani sub-basin, Andhra Pradesh: Significant Paleoproterozoic tectono-magmatic event in SW Part of the Cuddapah basin, Eastern Dharwar Craton; *J. Geol. Soc. India* **83(4)** 355–362.
- Satyanarayanan M, Balaram V, Sawant S S, Subramanyam K S V and Krishna G V 2014 *High precision multi-element analysis on geological samples by HR-ICP-MS*; In: Proceedings of 28th ISMAS Symposium and Workshop on Mass Spectrometry (eds Aggarwal S K, Jaisan P G and Sarkar A, ISMAS Secretariat, Mumbai, pp. 181–184, ISBN: 978-81-904442-7-9.
- Sen S N and Narasimha Rao C 1967 Igneous activity in Cuddapah Basin and adjacent areas and suggestions on the paleogeography of the basin; In: *Symposium on Upper mantle project*, GRB and NGRI Publ. **8**, pp. 261–285.
- Sheldon N D, Retallack G J and Tanaka S 2002 Geochemical climofunctions from North American soils and application to paleosols across the Eocene–Oligocene boundary in Oregon; *J. Geol.* **110(6)** 687–696.
- Sheppard S, Rasmussen B, Zi J W, Soma Sekhar V, Sarma D S, Ram Mohan M and McNaughton N J 2017a Sedimentation and magmatism in the Paleoproterozoic Cuddapah Basin, India: Consequences of lithospheric extension; *Gondwana Res.* **48** 153–163.
- Sheppard S, Rasmussen B, Zi J W, Soma Sekhar V, Sarma D S, Ram Mohan M and McNaughton N J 2017b U–Pb dating of metamorphic monazite establishes a Pan-African age for tectonism in the Nallamalai Fold Belt, India; *J. Geol. Soc. London*, <https://doi.org/10.1144/jgs2017-051>.
- Taylor S R and McLennan S M 1985 *The continental crust: Its composition and evolution*; Oxford, Melbourne; Blackwell Scientific Publications, ISBN: 0632011483.
- Totten M W, Hanan M A and Weaver B L 2000 Beyond whole-rock geochemistry of shales: The importance of assessing mineralogic controls for revealing tectonic discriminants of multiple sediment sources for the Ouachita Mountain flysch deposits; *Geol. Soc. Am. Bull.* **112(7)** 1012–1022.
- Totten M W and Blatt H 1993 Alteration in the non-clay mineral fraction of pelitic rocks across the diagenetic to low grade metamorphic transition, Ouachita Mountains, Oklahoma and Arkansas; *J. Sedim. Petrol.* **63** 899–908.
- Verma S P and Armstrong-Altrin J S 2013 New multi-dimensional diagrams for tectonic discrimination of siliciclastic sediments and their application to Precambrian basins; *Chem. Geol.* **355** 117–133.
- Walsh J P, Wiberg P L, Aalto R, Nittrouer C A and Kuehl S A 2016 Source-to-sink research: Economy of the Earth's surface and its strata; *Earth Sci. Rev.* **153** 1–6.
- Wronkiewicz D J and Condie K C 1987 Geochemistry of Archean shales from the Witwatersrand Supergroup, South Africa: Source-area weathering and provenance; *Geochim. Cosmochim. Acta* **51(9)** 2401–2416.
- Yang J, Cawood P A, Du Y, Li W and Yan J 2016 Reconstructing Early Permian tropical climates from chemical weathering indices; *Geol. Soc. Am. Bull.* **128(5–6)** 739–751.
- Zachariah J K, Rao Y B, Srinivasan R and Gopalan K 1999 Pb, Sr and Nd isotope systematics of uranium mineralised stromatolitic dolomites from the Proterozoic Cuddapah Supergroup, south India: Constraints on age and provenance; *Chem. Geol.* **162(1)** 49–64.

Corresponding editor: N V CHALAPATHI RAO